8-19-2011

# External Reforming SOFC Coupled with Biomass-to-Syngas Reactor

Amit Patel

*Santa Clara University*

**SANTA CLARA UNIVERSITY**

Department of Mechanical Engineering

Date: August 19, 2011

I HEREBY RECOMMEND THAT THE THESIS PREPARED
UNDER MY SUPERVISION BY

Amit Patel

ENTITLED

# External Reforming SOFC Coupled with Biomass-to-Syngas Reactor

BE ACCEPTED IN PARTIAL FULFILLMENT OF THE REQUIREMENTS
FOR THE DEGREE OF

**MASTER OF SCIENCE IN MECHANICAL ENGINEERING**

_____
Thesis Advisor

_____
Department Chairman

# External Reforming SOFC Coupled with Biomass-to-Syngas Reactor

By

Amit Patel

MASTER THESIS

Submitted in Partial Fulfillment of the Requirements for the
Master of Science Degree in
Mechanical Engineering in the School of Engineering
Santa Clara University, August 2011

Santa Clara, California

**TABLE OF CONTENTS**

## LIST OF TABLES

# LIST OF FIGURES

# ABSTRACT

This thesis introduces a thermodynamic model of an external reforming SOFC coupled with a biomass-to-syngas reactor in order to calculate energy and power that can be extracted from the fuel. Some of this energy will be used for electrical work and some of this energy will be used to provide heat to the reactor to drive the endothermic reactions occurring throughout the process. We analyzed four different feedstocks for their fuel cell heat dissipation and fuel cell power characteristic: pure syngas, pure carbon-derived syngas, coal-derived syngas, and biomass-derived syngas. Pure syngas consists of only CO and $H_2$ while the other three cases of syngas consist of CO, $H_2$, $H_2O$, $CO_2$, and $CH_4$. Pure syngas did not take the reactor into account.

The results of the analysis had shown that the absolute value of the Gibbs free energy of the fuel cell for pure syngas increased as the hydrogen concentration increased for temperatures above 1100 K. Opposite behavior occured for temperatures below 1100 K due to entropy change being less significant at lower temperatures. The results had also shown pure carbon-derived syngas to have the highest hydrogen concentration coming out of the reactor, which led to a higher Gibbs free energy of the fuel cell. This consequently led to a much higher maximum power density for any given temperature, followed by coal-derived syngas and biomass-derived syngas. Pure carbon-derived syngas also allowed the fuel cell to dissipate more heat than coal-derived syngas and biomass-derived syngas. Pure carbon was oxygen-free before the reactor and hydrogen-rich after the reactor, thus allowing for high overall performance. High oxygen content hindered the performance of biomass-derived syngas, thus requiring the incorporation of de-oxygenation in the reactor. Coal gives higher overall performance compared to biomass at the expense of excess burning of air in the reactor and excess ash emission.

# 1   INTRODUCTION

Sustainability is a path forward that allows humanity to meet current environmental and human health, economic, and societal needs without compromising the progress and success of future generations [1]. With the rising concern about greenhouse gas (GHG), many countries are pursuing efforts to develop more sustainable energy systems to replace conventional combustion heat engines. Solid oxide fuel cells (SOFC) are a great alternative to these combustion engines due to the simple fact that the fuel it uses is much cleaner than coal. These electrochemical devices are not limited to the Carnot efficiency, thus enabling efficiencies higher than traditional combustion-based thermal engines. Fuel-cell powered vehicles running on hydrogen have the potential of emitting zero emissions; this can ultimately significantly reduce the net emission of GHG if more people invest in this technology. Due to its high temperatures, an SOFC can also be thermally integrated with a bottoming cycle for power generation, as will be seen in sections to come.

The hydrogen used to fuel these SOFCs must come from a reliable and clean source. Biomass, a renewable energy source, is gaining popularity due to its availability in nature [2]. Biomass is an attractive fuel source for SOFC application because of its feasibility to be converted into syngas — a gas mixture containing high amounts of hydrogen and carbon monoxide. This conversion is typically carried out through gasification, which introduces the biomass with steam and/or oxygen at a very high temperature in order to extract usable fuel in the form of syngas and rid the biomass of unusable material. One example of a gasifier that converts biomass into syngas is the reactor created by Alyaser et al. [3]. This reactor uses its product, or syngas, as startup fuel for combustion with air

in order to heat the steam at a specific temperature so as to achieve the optimal hydrogen content in the final product made by the mixing of biomass and steam. The combustion of syngas with air provides energy to the endothermic reactions that occur in the fuel cell. The SOFC uses this final product, or syngas, for its hydrogen content, as will be seen in Chapters 3 and 4. Thus, the reactor uses the syngas it creates to fuel itself and the fuel cell.

A thermodynamic model of an SOFC coupled with a biomass-to-syngas reactor will be developed in order to calculate potential energy and power that can be extracted from the fuel cell. Some of this energy, which will be released in the form of heat, will also be calculated in order to examine the possibility of reducing the required combustions in the reactor. Through these combustion reductions, less startup fuel would have to be combusted with air in order to provide energy to the endothermic reactions in the reactor; the fuel cell will ideally provide heat for these reactions. Four different cases for this process will be carried out for this model:

     1)  The first and main case will deal primarily with syngas entering the fuel cell, or only carbon monoxide and hydrogen entering the anode. Since biomass is not completely carbon neutral, the other three cases will take a closer look at real values of reactor byproducts, which mainly consist of hydrogen, carbon monoxide, carbon dioxide, methane, and water. Thus, these elements will enter the anode side of the fuel cell. These other three cases will examine three different feedstocks for the reactor: pure carbon, biomass, and coal.

     2) Since the calculations that went into modeling the reactor [3] assume pure carbon as feedstock, this will be the second case to be examined. As opposed to real coal, pure carbon does not contain any volatile matter. Thus, it does not need to undergo devolatilization or partial combustion.

3) Biomass will be the third case to be examined in order to see how well this cleaner feedstock compares to coal

4) Coal will be the fourth case to provide a baseline for other feedstock

Before the scope of this thesis narrows into this area of SOFC coupled with a biomass-to-syngas reactor, the broader impact of the SOFC and its fuel must first be understood in terms of its sustainable impact.

## 1.1    Broader Impacts

### 1.1.1    Energy Sustainability of Hydrogen

The global demand for fuel increases as the global population increases day by day. Oil is a scarce commodity that cannot accommodate for this demand as it increases. Statistics show that growth in world population has resulted in an increase of 35% in world oil demand over the past 30 years. The conventional oil reserves may last only 25 years; a renewable means of fuel must be found [4]. Hydrogen is currently perceived as an attractive alternative to carbon-based fuels. Unlike carbon-based fuels, hydrogen is a renewable source similar to solar energy and biomass. The amount of energy released from the combustion of hydrogen is higher than that released by coal due to its lower heating value being up to 4x higher than that of coal [5]. The main distinction between hydrogen and carbon based fuel is that hydrogen is not a primary energy source [6]. It is an energy carrier that must be produced by another means of energy.

The current hydrogen economy encompasses three different areas: production, storage, and transportation. For this thesis, the hydrogen will be assumed to be directly fed into a solid oxide fuel cell. Since packaging and storage will not be an issue in this process, the

analysis of the hydrogen economy will be brief. As mentioned before, hydrogen is an energy carrier that must be generated from another source. There are many methods that are available on the market which are used to produce hydrogen. The most common and cheapest method is steam methane reformation. Although it is the cheapest method, significant amounts of carbon are still emitted into the atmosphere based on the fossil fuel being used. Storage is an area that needs much improvement. At STP, hydrogen gas is 3000 times larger in volume than an equivalent amount of gasoline. It can be compressed and cryogenically liquefied to allow for more compact storage, but at a cost: roughly 60% loss in energy [6]. Transportation isn't as big an issue as storage and production, especially if the hydrogen is liquefied. The main downside is that the cost of transporting hydrogen is about 15 times higher than an equivalent amount of liquid hydrocarbon fuel; this is due to hydrogen having a very high calorific value by mass but very low calorific value by volume [7].

Thus, much of the environmental problems arise in the production process. The environmental impact of hydrogen derived from fossil fuels can be linked to the process that is used to carry out the conversion of biomass into syngas. The reduction targets in greenhouse gases set by the Kyoto Protocol has not only influenced government to make more investments in cleaner technology and resources, but it has also influenced corporations to take part in this global endeavor. For example, Shell and British Petroleum has invested several billion dollars in the R&D and commercialization of the hydrogen energy [8]. Several demonstration projects have been made in order to bridge the gap between R&D and the commercialization level.

## 1.1.2    Biofuels and Sustainability

Biomass is a renewable energy source that harnesses the hydrogen and carbon from living or recently living things. An attractive feature of biomass is that it is very diverse in the sense that it can be found from many sources, including wood residue, organic waste, and animal waste. The current vision of the DOE's Biomass Program is a sustainable renewable energy solution that displaces fossil fuel, enhances energy security, promotes environmental benefits, and creates economic opportunities across the nation [9]. Thus, the sustainability of biofuel production depends on a spectrum of variables. One of the variables has to do with environmental sustainability. Although there is a reduction in the emission of carbon dioxide in burning biomass-based fuel, there is still a significant amount that is still being released into the atmosphere. One of the key benefits of biomass is that as it grows, biomass absorbs this carbon dioxide back from the atmosphere, thus allowing it to be recycled. Studies have shown that, based on the type of biomass-based fuel being used, greenhouse gas emissions can be reduced by as much as 86% [9]. This advantage, however, depends on the sustainability of both the agricultural and forestry sector of the biomass source. In order for there to be continuous utilization of a particular biomass source, the soil must be kept healthy. Sustainable soil health involves minimizing soil erosion, maintaining essential nutrients, and protecting the soil's physical and biological attributes [9]. Water quantity and quality must be maintained as well.

It should be noted that these biofuels are not completely carbon neutral. Many of the processes used in the production and maintenance of these biofuels results in the emission of other greenhouse gases. Carbon is ultimately released in machinery usage and the transport of the biofuel to its point of use. Another possible leakage of carbon dioxide can be attributed to the cutting down of a forest to grow biofuels. This huge initial release of carbon dioxide can take the biomass anywhere between 50-100 years to compensate. Nitrous oxide is also released through the use of fertilizer, thus adding to the

overall amount of greenhouse gases being released into the atmosphere. Thus, the actual carbon reduction of greenhouse gases depends on the way it is grown, where it is grown, and how it is converted from the feedstock into the biofuel [10]. Another drawback has to do with possible deforestation. As more and more rainforests are cut down, more carbon dioxide ultimately enters the atmosphere. For this reason, DOE has made larger investments in forest restoration and bio-refineries [9].

Another environmental impact of biofuel has to do with food security. In poverty-stricken nations, sustainability of biomass reaches a conflict between the environment and the economy. The diversion of arable land for food grown crops to the production of crops which are then burned for fuel is not beneficial for poor people that struggle for food. The demand of these biofuels from the U.S. thus raises the price for agricultural commodities. What might be beneficial to the economy can consequently be detrimental to a starving nation if the farmers are receiving higher returns on biofuel over food crops [10].

### 1.1.3   Economic viability

Biomass crops are currently used as feedstock for the production of electric power, liquid fuels, and chemicals. The main reason as to why the DOE did not fully advocate the production of biomass is because it used to be a niche market where electricity was expensive and fuel was cheap or incurred a disposal cost [2]. In order for biomass production to become workable with DOE's projected costs, there had to be:  1) an increase in fossil fuel prices, 2) rapid market development of biomass-based co-products, 3) and more efficient gasification and turbine systems for power generation. The first and second criterions have already been fulfilled; this thesis will help advocate the third criterion. In response to the current predicament of our polluted atmosphere, many countries around the world have shifted focus to biofuel industries. The production

6

and demand of these industries are primarily shaped through government policy, in response to the DOE, in terms of finance and regulation [12]. Fuel tax exemptions are being allocated by the government to companies that choose to produce biofuels in hopes of a more sustainable future. As mentioned before, the biofuel comes from the biomass that is grown in crops by farmers around the world. The main dilemma comes into play when farmers would rather produce biomass crops over food crops in order to receive a higher rate of return on their investment.

The chief economic setback of the biomass-based hydrogen economy is the production cost. This cost encompasses the capital equipment costs, feedstock cost, availability cost, transport cost, and operating costs. In order for there to be a better understanding of the production cost of biomass-based hydrogen, **Table 1-1** has been compiled by Balat et al. [13] illustrating optimistic production costs of hydrogen from various sources:

**Table 1-1:** Product cost of hydrogen from various sources [13]

| Method | $/kg |
|---|---|
| Steam methane reforming | 0.78 |
| Coal gasification | 1.41 |
| Hydrocarbon partial oxidation | 0.99 |
| Biomass gasification | 1.24 |
| Biomass pyrolysis | 1.26 |
| Electrolysis | 2.88 |
| Solar electrolysis | 4.29 |
| Photobiological production | 3.77 |

As can be seen in **Table 1-1**, steam methane reformation is the cheapest method available on the market. However, as mentioned before, carbon emissions for this method are significantly high and often times require sequestration [14]. Hydrocarbon is the next best alternative in terms of price, yet there still remains the underlying carbon emission problem. Biomass gasification and pyrolysis are thus shown to be the most overall

economically favorable processes for renewable hydrogen production. Several studies have shown that this production cost is strongly dependent on the cost of feedstock, which is relatively inexpensive.

## 1.2    Important Applications

### 1.2.1    Energy Grid: Cogeneration

Cogeneration, or combined heat and power (CHP), is a relatively clean and efficient approach to generating power and thermal energy from a single fuel source. The concurrent production of electrical and thermal energy has the potential to reduce primary energy consumption, greenhouse gas emissions, and air pollutants. Thermal energy is recovered from waste heat in order to provide water heating and space heating to any energy system, building, or facility. While the conventional method of producing usable heat and power separately has a typical combined efficiency of 45%, cogeneration systems can operate at levels as high as 90% [15]. These high efficiencies mainly stem from the utilization of the waste heat in order to reduce the energy loss that would otherwise ensue through the generation of power alone. It should be noted that the primary focus of this thesis is to utilize the SOFC not only for its electricity, but also for its waste heat in order to reduce thermal energy requirements of the biomass gasifier. Micro-combined heat and power systems integrated with PAFCs, or Phosphoric Acid Fuel Cells, comprise the largest market segment of existing CHP products worldwide, with SOFC still being in the prototype stage of development. The main competition of this combined technology is gas, oil, and electric furnaces. From a cost perspective, the capital cost of SOFCs does not make it a practical competitor. Studies have shown that if a small SOFC is run on constant power with an electric power output of 1-2 kW, then it is ultimately a competitor of electrical furnaces, but not by much. The high capital cost

8

along with high operational cost of SOFCs due to inflexibility to shutdowns and turn-offs does not make it a competitor to the gas heating system [16].

The main challenge with micro-cogeneration systems combined with SOFCs is that its theoretical electrical efficiency of 45% not only compares with its actual prototype electrical efficiency, but it does not come close to actual efficiencies up to 55% that can be attained by combined cycle central power plants [17]. Due to this, SOFCs have yet to transition from the prototype stage to commercialization. On the larger scale, however, it is anticipated that efficient natural gas fuel cell technology will offer an economically and environmentally attractive alternative to both combustion cogeneration plants and centralized power generation [18]. These economic incentives are essentially seen by the customer in the form of cost incentives and rebates through the renewable energy policies being established by government on both the state and federal level. Credit is also possible by selling excess energy back to a utility grid.

### 1.2.2 Off-Grid

Remote homes near rural industries are typically too far away from public utilities; they cannot rely on municipal water supply, natural gas, electrical power grid or similar utility services. The people who live in these homes typically generate their electricity through renewable means of energy, such as solar or wind. As long as there is an electrical generator and a fuel reserve other than diesel, the environmental impact of these homes are kept much lower than the homes that rely on the energy grid. Just like these independent homes, data centers also rely on independent power sources. This idea of reserved power has also been implemented into current data centers through the use of a UPS, or uninterruptible power source. Dips, single-phase disruptions, and outages are becoming a serious concern for the economic future of the country's high tech industries

because a power outage could mean heavy losses in productivity or risks of damaging equipment. Thus, these UPSs provide backup power to a load when the input lines to the public utilities fail. SOFC-based UPS technologies are still in the development stage due to the reoccurring issue of storage of sufficient hydrogen gas to supply a high load at 65% conversion efficiency for at least 8 hours of service [19]. Thus, many developers have chosen to extract hydrogen from more viable sources of fuel, including methane.

As mentioned before, fuel reserves are required for autonomous homes to remain independent of the grid. Many remote areas currently employ photovoltaic with battery storage for backup [20]. The problem with this cycle is that the batteries can only store energy for a relatively short amount of time and requires replacement after a few years. Hydrogen storage, on the other hand, can provide low loss backup for longer periods and never has to be replaced. One study [20] in particular had shown that the replacement of the battery with a PEM fuel cell, PEM electrolyser, and hydrogen storage had provided not only a volumetric advantage, but also a reduction in the overall carbon footprint. An electrolyser is a device that uses electrolysis in order to convert water into hydrogen. The photovoltaic provides direct energy to the home during the day. Excess energy would be fed to the electrolyser to be converted into hydrogen and stored for evening use by the fuel cell when power load is much less. Since hydrogen storage is very inefficient in today's economy due to hydrogen gas being 3000 times larger in volume than an equivalent amount of gasoline, many developers are trying to reduce the requirement of hydrogen fuel reserves by combining the fuel cell with other renewable sources of energy.

## 1.3    Alternative Technologies

The hydrogen economy is not currently the dominant source of fuel; coal is. Due to this, coal-derived syngas along with coal itself and the technologies that use this coal will be discussed in this section. The fuel cell will first be compared and contrasted to the internal combustion engine and power plants. We will then go one step further and discuss alternative means of deriving syngas through coal gasification.

### 1.3.1 Electricity Generation from Fuels

#### 1.3.1.1 Internal Combustion Engine

This thesis mainly concerns fuel cells in stationary applications. However, the fuel cell has many more applications, including moving applications. The fuel cell is ultimately a means of using the fuel it is given in order to provide electrical power to an external source. Given that fuel cells are targeting the transportation market, the power capabilities of a fuel cell will be compared to the internal combustion engine to give the reader a more clear understanding of the technological advances in the fuel cell market.

If the hydrogen economy replaces the current fossil fuel economy, our means of transportation will change as well. The power supply of boats, cars, and airplanes currently comes from the use of the internal combustion engines, or ICEs. The only similarity between a fuel cell and an ICE is that they generate power from a fuel, and the main difference between these two entities is the way the fuel is used. Advantages of the fuel cell over the ICE are that it can achieve efficiencies up to 2-3 more than an ICE and it is quieter due the simple fact that there are no moving parts in a fuel cell [21]. This high efficiency can be attributed to the fuel cell being able to extract more power out of the same quantity of fuel when compared to traditional combustion power of gasoline. ICE's

11

operate at high temperatures of about 2300° C, while SOFCs usually operate at a range between 800° C to 1000° C [22]. Apart from the obvious advantages between these two power generators, there are also inherent disadvantages. The cost of an ICE is $50/kW of capacity while the cost of a hydrogen fuel cell is about $1500-3000/kW [22]. Until this cost barrier is reduced, there is no cost incentive for a potential customer to purchase a fuel cell operated vehicle. The main purpose of this section is to relate a fuel cell with an ICE. Thus, it will be left to the reader to research the functionality and other related areas of the ICE.

In order for the reader to fully realize the environmental impact of both a fuel cell vehicle and an ICE, a life cycle assessment must be carried out. The life cycle of a vehicle consists of the total emissions related to the production, assembly, distribution, maintenance, and disposal of the vehicle. In order to get an idea of this life cycle comparison between a fuel cell and an ICE, we summarized the work of Zamel et al [23]. Results had shown that the material production had contributed the most carbon emissions related to thermal energy and electricity generation when compared to the other steps in the vehicle life cycle. This material production stage was strongly dependent on the weight of the material being used. The fuel cell vehicle was shown to use 2x the amount of copper and 1.5x the amount of other materials than an ICE. The total result of the energy consumption of the future life cycle of an ICE had shown that it was about 4 GJ less than that of a fuel cell vehicle, or FCV. This study did not take into account the actual operational use of both vehicles. This extra factor would have shown that carbon emissions from an ICE would have greatly outweighed carbon emissions from the material production step in the FCV life cycle.

### 1.3.1.2  Power Plant

Power plants have been around for a long time due to advances in the technology it currently uses. For example, larger and more efficient steam turbines and electric generators have made large power plants more convenient for power generation. Another favorable characteristic about them is that the fuel it uses is currently abundant in nature. In a typical coal combustion-based power plant, heat from coal being burned in the boiler furnace is used to boil water in the boiler, making steam that drives a steam turbine-generator. In the burning of coal in the furnace, carbon dioxide is also emitted into the atmosphere. These power plants are currently the largest producers of carbon dioxide [24]. In some coal combustion-based power plants, only a third of the energy value of coal is actually converted into electricity. Thus, pollution outweighs the amount of energy being extracted from these fossil fuels. Many methods exist that improve on the efficiency of these fossil fuel power plants, one of them being coal gasification, as will be explained in Section 1.3.2. Another method would be to co-fire the fossil fuel with a carbon neutral fuel, like biomass, to mitigate the global warming problem.

One of the direct benefits of co-firing is that existing plants can use other fuels that might be cheaper and/or environmentally friendly. The technological feasibility and future commercial prospect of biomass co-firing with coal is a feasible and effective technology for reducing greenhouse gas emissions, particularly sulfur and mercury, using existing coal-fired plants [25]. Tests and demonstrations have shown that co-firing coal with low percentages of biomass can raise the electrical efficiency up to 37% from 15% [26] and keep the system stable. As will be seen in Chapter 2, the main barrier preventing the use of biomass is the cost related to fuel supply. Factors that affect fuel supply include climate, closeness to population centers, and dependable supply. Another issue that must be addressed has to do with co-firing coal with high percentages of biomass, which leads to instability of the system. This instability can be attributed to the biomass ash containing reactive salt compounds that have the potential to create slagging or fouling in

the combustor [27]. These percentages can be controlled if the fuel-handling and feed equipment of the current coal power plant are retrofitted to meet the needs of biomass. Thus, this is one of the many options available that requires the least amount of change while still significantly reducing the carbon footprint of current coal fired power plants.

## 1.3.2    Syngas Generation: Coal Gasification

### 1.3.2.1    Integrated Gasification Combined Cycle

Coal gasification is a much cleaner way of converting coal into a product of energy. Instead of burning coal directly, gasification breaks down coal into its chemical constituents. The environmental benefits of gasification stem from the capability to achieve extremely low levels of $SO_x$ and $NO_x$ and particulate emissions from burning coal-derived gases, thus furthering national goals to protect the environment. This is done by introducing coal to superheated steam and controlled amounts of air under high temperature and pressure. Chemical reactions ensue and eventually produce a mixture of CO, $H_2$, and other gaseous chemical substances. IGCC, or integrated gasification combined cycle, is a technology that uses coal gasification through the utilization of two turbines. The coal gases mentioned earlier are fired in a gas turbine to generate one source of electricity while the exhaust gases from this gas turbine and the gasification process itself are used to generate steam for use in a steam turbine-generator. This dual source of electricity can potentially boost fuel efficiency up to 50% or more [28], thus making it an attractive source of electricity without having to change the feedstock. The flexibility of an IGCC allows it to also convert any carbon based feedstock, including waste and biomass, into any type of product, including fuels such as hydrogen. In terms of versatility, this feedstock and product flexibility gives IGCC dominance over other gasifiers that are confined to a single feedstock and product. This flexibility, along with

the fact that coproduction of hydrogen has an incremental cost less than 10% of the initial IGCC plant cost, gives the IGCC the potential to be the backbone of the hydrogen economy in the future.

The main setback of an IGCC plant, as with many other clean technologies, is cost. The capital cost for a natural-gas combined cycle is currently about one-half the cost of a coal IGCC plant [29]. In order for power plants to integrate with the IGCC, there has to be a matching economy to scale as well as fuel cost advantages. Nevertheless, the DOE believes that by 2015, efficiency of an IGCC will be above 60% and capital cost will be about 58% lower than its present capital cost [29]. The DOE is currently investing into R&D programs to expand its scope of demonstration projects to incorporate fuel cells as well, as will be seen in the next section.

## 1.3.2.2  IGFC

The main purpose of this report is to examine SOFC power characteristics and heat output based on syngas input. In an integrated gasification fuel cell, or IGFC, coal is the typical fuel used in the production of syngas. IGFC combines coal gasification technology with an SOFC in hopes of achieving DOE's goal of 60% electrical efficiency while separating 90% of the evolved CO2 amenable to sequestration [30]. Methods used to help IGFC achieve these goals include using efficient catalytic hydro-gasifiers and direct internal reformation of methane. The main barrier preventing coal gasification coupled with an SOFC from achieving high efficiency numbers similar to that of biomass gasification coupled with SOFC has to do with carbon dioxide sequestration. Thus, electrical efficiency of the IGFC is strongly dependent on the gasifier being used. Higher electrical efficiencies would be achieved if there was not a need to remove the carbon from the atmosphere.

In addition to higher efficiencies and more efficient carbon sequestration, IGFC's have other advantages compared to a conventional IGCC. The raw water usage of an IGFC plant is about half that of an IGCC when wet cooling towers are employed for plant heat rejection. Since no high temperature combustion of fuel with air takes place, there are virtually no nitrogen oxide emissions produced by an IGFC [30]. It should be noted, however, that these aforementioned disadvantages might be alleviated through the coupling of an IGCC with a fuel cell, which is still being researched by DOE. These cleaner technologies have yet to be adopted due to the repeated cost barrier that continually arises.

## 2    BACKGROUND

We will now shift focus towards the properties, functionality, and basic procedure of three different entities directly relating to this thesis: the biomass feedstock, the biomass-to-syngas reactor, and the solid oxide fuel cell.

### 2.1    Biomass and Bio-oil

Before the methodology behind the primary objective is introduced, it is best for the reader to understand the overall process. A diagram for the analysis of this thesis can be seen in **Figure 2-1:** , with biomass being the starting point of the procedure:
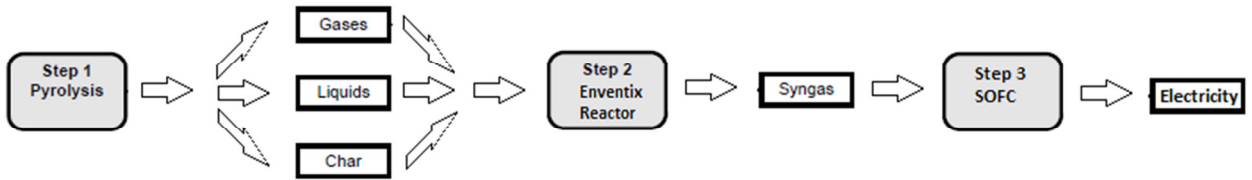
**Figure 2-1:** Conversion of biomass to electricity. Pyrolysis is executed in order to rid the biomass of volatile matter and charcoal. This volatile matter, or bio-oil, is fed into the reactor, which further rids the volatile matter of char. The combination of combustion and gasification in the reactor converts this carbonaceous feedstock into syngas. This syngas, which is high in hydrogen and carbon content, is fed into the SOFC to produce electricity with carbon dioxide and water as byproducts.

Biomass is often times used to create bio-oil and syngas through pyrolysis. Syngas is a non-condensable gas consisting collectively of hydrogen, carbon dioxide, carbon monoxide, and light molecular weight hydrocarbon gases [31]. Bio-oil comprises of condensable vapors that normally contains very high levels of oxygen. Pyrolysis, which is an endothermic process, has mainly to do with the process before combustion. Pyrolysis is the initial process that takes place when organic matter is first heated in the absence of oxygen to produce combustible gases. Pyrolysis at high temperatures decomposes biomass into charcoal and other volatile matter. This volatile matter takes the form of bio-oil at room temperature and syngas at much higher temperatures. In order for more syngas to be produced, the pyrolysis process must not only be a precursor to combustion, but also gasification at high temperatures. Biomass gasification is the conversion of a carbonaceous feedstock by partial oxidation into a syngas consisting primarily of hydrogen and carbon monoxide. The biomass-to-syngas reactor analyzed in this thesis does not incorporate partial oxidation like other gasifiers do; steam reformation is executed through the combustion of syngas with air. This steam reformation is employed to the bio-oil in order to maximize hydrogen and carbon monoxide concentration and reduce hydrocarbon aromatics and carbon deposits. This syngas then

travels to the SOFC, where electricity is produced along with carbon dioxide and water as byproducts.

## 2.1.1  Thermochemical and Physical Properties

Bio-oil has an elemental composition similar to that of its parent, biomass. Unlike coal, the elemental composition of biomass has a low content of carbon and ash. Like coal, however, this renewable fuel has inherent disadvantages as well.  A disadvantage of bio-oil is that it has a lower heating value of about $26 \frac{MJ}{kg}$ when compared to that of fossil fuel, which has about 42-44 $\frac{MJ}{kg}$  [31]. This lower heating value thus prevents it from releasing more heat during combustion. Another disadvantage is that it is highly acidic, thus making it very difficult to transport and store. This is the main reason as to why bio-oil is often encased in stainless steel containers. However, it does have the added advantage of emitting less nitrogen emissions, thus lowering a small portion of greenhouse gases. The specific gravity of bio-oil is typically larger than water and the original biomass, thus making it heavier after the pyrolysis process. Typical bio-oil contains 55%-64% C, 5%-8% $H_2$,  27%-40% $O_2$, 0.05%-1.0% $N_2$, and 0.03%-0.30% Ash [31]. Thus, it isn't uncommon for most biomass feedstocks to have significant amounts of nitrogen and ash that can potentially pose a threat to the machinery being used to process it. Based on the aforementioned elemental composition and assuming a 60% yield of water-free bio-oil from biomass, 12–13 kg of hydrogen can potentially be produced from 100 kg of biomass [31]. This low yield of about 8% is mainly dependent on the specific feedstock being used, as will be seen in the next section.

## 2.1.2  Feed-stocks Comparison – Pros and Cons

The most common types of biomass, which will be examined in this section, are wood, straw, and bagasse. About 21 million metric tons of bagasse, which is fibrous matter that remains after sugarcane stalks are crushed, is produced as by-product per year. Heat produced by combusting the bagasse is typically used for steam generation and energy use in other sugar industry sectors [32]. Due to their high moisture content, there are typically dried prior to the pyrolysis process to reduce moisture content of bio-oil. Straw, on the other hand, is an agricultural byproduct of wheat. Without straw, most people today would not have cereal to eat for breakfast. Wood comes directly from plants. They are typically used for applications other than fuel, such as construction and furniture. As mentioned before, the environmental impact of using wood is dependent on the method used to attain it. For example, the chopping of an entire tree can result in massive amounts of carbon dioxide being released into the atmosphere all at once. **Table 2-1** will be the foundation for what is to be discussed in this section:

**Table 2-1:** Analyses of selected biomass material [32]

| | C | H | N | S | O | Cl | Ash | Volatile matter | Fixed carbon |
|---|---|---|---|---|---|---|---|---|---|
| **Bagasse** | 44.8 | 5.4 | 0.4 | 0.01 | 39.6 | - | 3 | 69 | 29 |
| **Wood** | 50 | 6 | 0.3 | - | 42.4 | - | 0.5 | 80.2 | 19 |
| **Straw** | 41.8 | 5.5 | 0.7 | - | 35.5 | 1.5 | 13.7 | 66.3 | 21.4 |

As can be seen in **Table 2-1**, bagasse has the highest carbon content with respect to the other biomass materials. Much of this fixed carbon, which converts to char, is often difficult to vaporize, even at temperatures as high as 1000° C [32]. Nonetheless, when it does vaporize, the carbon based non-condensable gases are typically CO, $CO_2$, $CH_4, C_2H_4$, and propane [32]. The straw has a high content of chlorine, an element which is very undesirable in power plant fuels. The amount shown in the table exceeds the

chlorine content of various coals, which can result in corrosion in the machinery being used to process the biomass. Straw also has the highest content of ash, which is directly related to ignition and combustion problems [33]. Based on **Table 2-1**, wood has the most volatile matter content out of the three, thus allowing for a higher bio-oil yield. Although it has less ash and virtually no chlorine, it still has the highest amount of carbon. Thus, higher contents of CO and $CO_2$ are more likely to develop after gasification. Nonetheless, it is common to see power plants using wood, the oldest type of fuel known to man, over other types of biomass to be co-fired with coal.

## 2.2    Pyrolysis Processing of Biomass

As mentioned before, pyrolysis is a form of incineration that chemically decomposes organic materials by heat in the absence of oxygen. These organic materials are transformed into gases, small quantities of liquid, and solid residues containing carbon and ash. As mentioned before, some biomass materials are volatile. This results in the act of thermal desorption, which is the removal of an absorbed or adsorbed substance [34]. The products of biomass pyrolysis include biochar, bio-oil, syngas, carbon dioxide, and methane. The content of gaseous and solid material depends on the final temperature and thermal environment. Steam reformation is used in the gasifier in order to achieve the desired hydrogen and carbon content of the final syngas byproduct.  As mentioned before, this is an endothermic process; heat transfer is a critical area in pyrolysis. Pyrolysis is dependent on both the particle size and moisture content of the feedstock [35]. Small moisture content can result in formation of only dust while large particle sizes will not allow rapid heat transfer through the particle. There are currently two types of pyrolysis: fast pyrolysis and slow pyrolysis. Slow pyrolysis takes several hours to complete with biochar as the main product while fast pyrolysis takes seconds to complete with higher yields of bio-oil and syngas. For this analysis, it will be assumed that fast

pyrolysis is being executed to produce more viable feedstock for the biomass-to-syngas reactor. For fast pyrolysis, a rapid rate of cooling and heating are required to minimize the potential for secondary reactions. These secondary reactions often result in reduction of quality and liquid yield [36].

## 2.3    Gasification Process

Pyrolysis is the precursor to combustion, which is subsequently the precursor to gasification. Gasification is the conversion of a carbonaceous feedstock to syngas at high temperature through the reaction of the raw material with oxygen and/or steam. The production on syngas occurs through the partial combustion of solid fuel, in this case biomass, at temperatures as high as 1000° C. As mentioned before, the biomass-to-syngas reactor analyzed in this thesis does not incorporate partial combustion; startup fuel or syngas is combusted with air to provide heat for gasification. The composition of the product gas depends mainly on the fuel, gasifier type, and gasification agent. For this thesis, the fuel will be varied between coal, biomass, and pure carbon. Complete combustion generally contains nitrogen, water vapor, carbon dioxide, and oxygen [37]. Incomplete combustion, which occurs when there is a surplus of solid fuel, generally contains combustible gases like hydrogen and carbon monoxide.

There are four distinct process involved in most gasifier designs: drying of the fuel, pyrolysis, combustion, and gasification. Higher than usual levels of moisture in the feedstock raises the energy requirement for evaporation in the gasifiers. These high moisture levels causes the reaction temperature to decrease, which results in poorer product gas with higher levels of tar [38]. Due to this fact, forced drying of the biomass becomes necessary in such systems. In these driers, the medium needed to dry the solid may be selected as pure vapor or a mixture of vapor and non-condensable gas or

combustion products [39]. In the case of SOFC, hot exit gas streams of the fuel cell may be circulated to the drier to reduce the moisture of the biomass.

Once the bio-char and volatile products are extracted from biomass through pyrolysis, combustion becomes the next step in gasification. In partial combustion, carbon dioxide is obtained from carbon in the volatile products and bio-char from pyrolysis and water is obtained from hydrogen. The combustion reaction is overall exothermic, as can be seen in **Equations 1 and 2**:

$$C + O_2 = CO_2 \ (+ \ 393 \ \text{MJ/kg mole}) \hspace{3cm} \textbf{Equation 1}$$

$$2H_2 + O_2 = 2H_2O \ (- \ 242 \ \text{MJ/kg mole}) \hspace{2.5cm} \textbf{Equation 2}$$
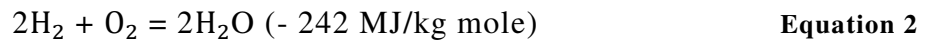
Thus, this reaction of carbon with oxygen assists in the endothermic reactions that take place in other reactions in the gasifier. The products of partial combustion, as can be seen above, eventually pass through a hot charcoal bed where the following reactions [37] take place.

$$C + CO_2 = 2CO \ (- \ 164.9 \ \text{MJ/kg mole}) \hspace{2.5cm} \textbf{Equation 3}$$

$$C + H_2O = CO + H_2 \ (- \ 122.6 \ \text{MJ/kg mole}) \hspace{1.8cm} \textbf{Equation 4}$$

$$CO + H_2O = CO_2 + H_2 \ (+ \ 42 \ \text{MJ/kg mole}) \hspace{1.8cm} \textbf{Equation 5}$$
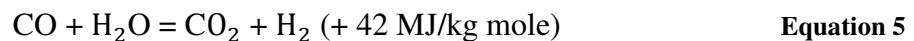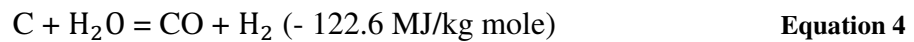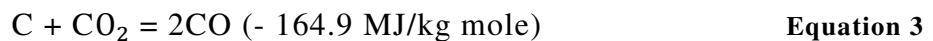
**Equation 3** is known as the Boudouard reaction. Its primary outcome rids the gasifier of excess carbon dioxide by combining it with the leftovers of the pyrolysis products in order to form carbon monoxide. **Equation 4** is known as Steam-Carbon reaction, which is carried out to increase the hydrogen and carbon monoxide in syngas while simultaneously reducing the carbon content. The water gas shift reaction is shown in

**Equation 5**, which is favored due to the fact that it is not only exothermic, but it also increases the hydrogen content of the syngas. It should be noted that this reaction is sensitive to temperature; the reaction shifts towards the reactants at higher temperatures. It is also not uncommon for there to be significant amounts of methane in syngas at lower temperatures. In cases like this, steam methane reformation is typically carried out by combining methane with steam to produce carbon monoxide and hydrogen. The only downside to this reformation is that the reaction itself is strongly endothermic. Thus, gasifiers are typically kept at temperatures that make methane content insignificant. Nevertheless, the final ideal product of the gasifier is a hydrogen rich syngas with low amounts of carbon monoxide.

## 2.4    Biomass-to-Syngas Reactor:

The reactor [3] that is to be analyzed for this thesis was created by Alyaser et al. It effectively executes the use of steam gasification of carbonaceous feedstock by indirectly heating the reacting flow through high temperature heat exchangers. The function of these heat exchangers is to heat up incoming water through the combustion of fuel and air. The main difference between this gasifier and other gasifers on the market is that there is virtually zero combustion with oxygen, thus preventing the production of poor quality products. Air separation is not required due to its decoupling of the heat source from the gas synthesis reaction. This means that heat produced at some parts of the reactor are used to drive the endothermic reactions at other parts of the reactor, thus lowering energy losses that are normally seen in other gasifiers that require partial combustion with oxygen. The main goal of this reactor is to reduce emissions and increase efficiency by incorporating combustion of startup fuel, or syngas, with air as

23

opposed to relying on partial combustion. **Figure 2-2** shows a detailed schematic created by Alyaser et al [3].
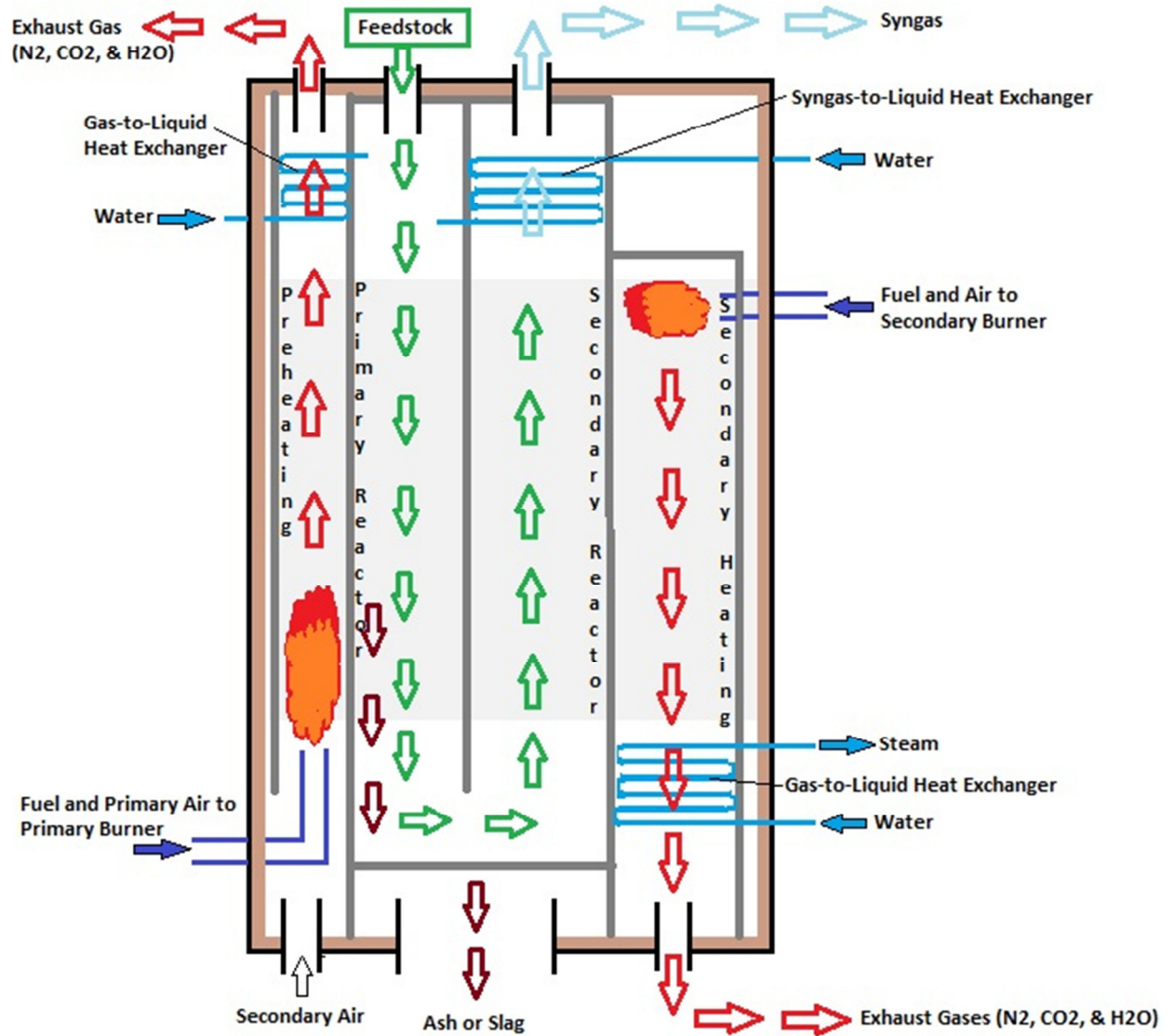


**Figure 2-2:** Schematic Diagram of biomass-to-syngas reactor [3]. Feedstock is fed into the reactor and continually mixed with steam at different temperature levels in order achieve desired syngas composition. There are 4 parts to the reactor: the pre-heating zone, the primary

reactor, the secondary reactor, and the secondary heating zone. The combustion of fuel with air provides heat for the endothermic reactions taking place in the gasifier.

### 2.4.1   Reactor Functionality

### 2.4.1.1  Pre-heating Zone

In order for the feedstock to convert into syngas, it must be continually mixed with high temperature steam until the desired concentration levels are reached. There are 4 parts to the reactor: the pre-heating zone, the primary reactor, the secondary reactor, and the secondary heating zone. As can be seen in **Figure 2-2**, the shaded grey area is separated into 4 pathways. Each pathway represents the aforementioned 4 parts of the reactor in numerical order. In the first pre-heating stage, water is fed into a gas-to-liquid heat exchanger that is heated up to steam through the combustion of fuel with air. Temperatures up to 1800°C are reached in this zone. This combustion of fuel with air thus drives the endothermic chemical reaction in the reactor core, where the superheated steam mixes with the feedstock that is fed into the primary reactor at a different location. The pre-heating zone has a high surface area to volume ratio to effectively transfer heat to the primary reactor and secondary heating zone to ultimately accelerate gasification.

### 2.4.1.2  Primary Reactor

Since devolatilization of feedstock begins to occur in a temperature range of 350-800°C, the primary reactor is maintained at a temperature below 1000°C. The purpose of the primary reactor is to separate and remove the inorganic solids from the gaseous mixture in the form of ash or slag before it enters the secondary reactor, as can be seen in

**Figure 2-2**. Once the mixture has reached the secondary reactor, which is kept at a temperature above 1260°C, the syngas is driven further to completion through the removal of methane, water, and carbon dioxide. Thus, the concentrations of hydrogen and carbon monoxide are increased to provide higher quality syngas to the fuel cell. Since the secondary reactor has a high surface area to volume ratio, it is able to efficiently receive a higher amount of heat from both the primary reactor and secondary heating zone.

### 2.4.1.3 Secondary Reactor/Secondary Heating Zone

In the secondary heating zone, air is again combusted with fuel to produce heat for the primary and secondary reactors. Additional superheated steam is generated by the secondary heat exchanger to ultimately mix with the gaseous mixture to achieve the desired concentration levels. Like the primary and secondary reactors, this zone also has a higher surface area to volume ratio to facilitate more efficient heat transfer to the reaction zones. Steam and exhaust gases are released into the atmosphere.

The main variables for this reactor are feed rate, water flow rate, and fuel flow rate. Each of these variables are adjusted through the use of sensors and computer-controlled instruments until the desired concentration levels are achieved. The endothermic reactions that are required in the reactor will be alleviated through the heat that is released by the fuel cell, thus reducing the amount of fuel needed to combust with air in order to heat the water into steam. Thus, the heat from the fuel cell will ultimately reduce the required amount of heat needed for the conversion of biomass into syngas.

### 2.4.1.4 Heat Assistance from SOFC

As mentioned before, biomass with high moisture can result in low efficiency. Thus, hot exit gas streams of the fuel cell may be circulated to the drier to reduce the moisture of the biomass. The overall electrochemical reaction for the fuel cell is exothermic. However, the endothermic reactions occurring in the reactor require energy in order to reduce the amount of fuel needed to combust with air. Thus, the goal of this system is to not only theoretically calculate the amount of electrical work being generated by the SOFC, but to also calculate how much heat can be sent over to the reactor from the fuel cell. Once all of the voltage losses are accounted for, the total voltage can be calculated. Since the total energy output takes the form of either electrical work or heat, one can simply subtract the electrical work from the energy input to get the heat dissipated for the SOFC. Any amount of fuel that is saved from combustion can ultimately reduce the GHG emissions from the exhaust pipes of this reactor. Another advantage is that the syngas that would normally be circulated for combustion would be transferred to the fuel cell instead, thus increasing the amount of syngas entering the SOFC.

## 2.4.2  Typical Applications

Typical application of any biomass gasifier includes the generation of power, fuel for transportation, and chemical synthesis. The derivation of syngas varies from gasifier to gasifer, mainly depending on reactor type, feedstock, and processing conditions. The main application of the product gas from the gasifier for this thesis is to generate heat and power. Apart from fuel cell application, these product gases can be injected into the combustion zone of the coal boiler of a co-firing plant. Percentages up to 10% are feasible without the need for substantial modifications to the coal boiler [40]. Product gases can also be fired in the gas engines of a CHP plant, resulting in $\frac{1}{3}$ electricity and $\frac{2}{3}$

27

heat. The technical challenge of this integration is the removal of tar, which can be detrimental to the entire process.

The product gases can also be used in the transportation sector of our economy through the formation of synthetic fuels and methanol. Synthetic fuels such as gasoline and diesel can be produced from synthesis gas via the Fischer-Tropsch (FT) process. The FT synthesis involves the catalytic reaction of H2 and CO to form hydrocarbon chains of various lengths [41]. The FT process can be used to produce either a light synthetic crude oil and light olefins or heavy waxy hydrocarbons [40]. The synthetic crude oil can be hydrocracked to produce diesel fuel, lube oils, and naphtha, which is an ideal feedstock for cracking of olefins. Methanol, on the other hand, is currently produced on an industrial scale exclusively through the catalytic reaction of carbon monoxide and some carbon dioxide with hydrogen [40]. Both reactions are exothermic, thus allowing the excess heat to be used in another application.

Chemical synthesis has a wide variety of applications, including the production of ammonia and hydroformylation of olefins. A major share of the ammonia that is made is used for fertilizer. The ammonia synthesis is a catalytic reaction between nitrogen and hydrogen. Two significant characteristics about syngas-based ammonia are that high concentrations of nitrogen are acceptable and the sum of the concentrations of carbon dioxide and carbon monoxide should be kept low [40]. Aldehydes and alcohols are produced through the hydroformylation of olefins on both an industrial and commercial scale. Hydroformylation is generally an exothermic, homogeneously catalyzed liquid-phase reaction of the olefin with hydrogen and carbon monoxide [40]. Thus, biomass gasifiers can be used in a wide range of applications other than power generation.

### 2.4.3   Alternative Biomass Gasifier Designs

There are many other types of biomass gasification technologies for hydrogen production that have been documented. Many of these gasification reactors extend beyond the scope of this thesis, which is why focus will be placed on reactors that most closely resemble the characteristics of the reactor used for this thesis. They can be classified into four major groups: fixed-bed updraft, fixed-bed downdraft, bubbling fluidized-bed and circulating fluidized bed. Since the fuel flows down in the reactor, only two of the gasifiers will be analyzed: the updraft gasifier and the downdraft gasifier. The main difference between the reactor and the two gasifiers mentioned above is that oxidant is not introduced to the feedstock in any part of the reactor used for this thesis. The role of oxidant is to combust with fuel in order to convert water into steam.

### 2.4.3.1 Updraft Gasifier

Just like the reactor, the biomass or bio-fuel is introduced at the top of the updraft gasifier. In the updraft gasifier, however, air and steam are introduced below the grate, which is below the gasifier, and moves up through the bed of biomass and char. Complete combustion of the char takes place at the bottom of the reacting bed; $CO_2$ and $H_2O$ are liberated at this point. These hot gases (~1000° C) are passed through the bed above and are reduced to CO and $H_2$ while rapidly being brought to a lower temperature (~500° C) [42]. The main advantage of this gasifier is that it is able to handle biomass with high moisture content. As mentioned before, the most common types of biomass tend to have high moisture content. Since some gasifiers, like the downdraft gasifier, cannot handle this amount of moisture, they are often dried during the pretreatment stage. The main disadvantage of this gasifier is that it has a high sensitivity to tar, which can result in damaging of processing equipment [43]. The downdraft gasifer, on the other hand, has a low sensitivity to tar.

## 2.4.3.2  Downdraft Gasifier

The downdraft gasifier has the same configuration as the updraft gasifier. The main difference is that oxidant and product gases flow down the reactor in the same direction as the feedstock. Another difference is that that the syngas leaves at a higher temperature than the updraft gasifier. Finally, there is virtually less than 1% tar in the syngas output compared to the syngas carrying 10-20% tar by weight in the updraft gasifier. The main disadvantage of this gasifier is that it is not feasible for small particle sizes [43]. As mentioned before, heat transfer is much more rapid when the particle size is made as small as possible. Thus, in this gasifier, the process of converting biomass into syngas takes much longer.

## 2.4.4  Chemical Equilibrium Composition

As mentioned before, four different feedstocks will be examined for this thesis. For the case of pure syngas, however, the reactor byproduct will consist of only $H_2$ and CO. The byproduct of the reactor for biomass, coal, and pure carbon will consist of $H_2$, $H_2O$, CO, $CO_2$, and $CH_4$.  As mentioned before, the composition of the syngas leaving the reactor is dependent on temperature, pressure, and composition of the feedstock. In order to calculate the equilibrium composition, the equilibrium constant must be calculated. The overall chemical equation must first be balanced in order to find the amount of moles, $n_i$, of the product in terms of the given amount of moles of the reactants. This can be seen in **Equation 6**:

$$n_A A + n_B B \leftrightarrow n_C C + n_D D \qquad \textbf{Equation 6}$$

where *A* and *B* are the reactants and *C* and *D* are the products. If the amount of moles of the reactants is known, then the amount of moles, $n_C$ and $n_D$, of the products must be found in terms of $n_A$ and $n_B$. The total number of moles, *n*, of the mixture is equivalent to the summation of $n_A, n_B, n_C, and\ n_D$. The molar fraction of each species is thus given as $y_i = \frac{n_i}{n}$. The stoichiometric coefficients, $v_i$, are related to the changes in the amounts of the individual species, as can be seen in **Equation 7**. This consequently allows us to calculate the equilibrium constant *K* with pressure in terms of atm, as can be seen in **Equation 8**.

$$\frac{-dn_A}{v_A} = \frac{-dn_B}{v_B} = \frac{dn_C}{v_C} = \frac{dn_D}{v_D} \qquad \textbf{Equation 7}$$

$$K(T) = \frac{y_C^{v_C} y_D^{v_D}}{y_A^{v_A} y_B^{v_B}} (P)^{v_C + v_D - v_A - v_B} = \exp(-\frac{\Delta G}{RT}) \qquad \textbf{Equation 8a}$$

where *P* is the pressure, $\Delta G$ is the change in the Gibbs function for the reaction given by **Equation 6**, *R* is the universal gas constant, and *T* is the temperature. The Gibbs free energy will be explained in detail in section 2.5.2.1. Thus, in order to calculate the chemical equilibrium composition, the total Gibbs energy given by **Equation 8a** must be minimized subject to atomic balancing of **Equation 6**. For example, if the unknown products $n_C$ and $n_D$ are found in terms of the known reactants $n_A$ and $n_B$, then the products can be introduced into the minimization of **Equation 8a** using Lagrange multipliers: $\lambda_1$ and $\lambda_2$. The extended form of **Equation 8a** can be seen in **Equation 8b**.

$$\min_{n_i, \lambda_p} \left(-\frac{\Delta G}{RT}\right) = \ln(K) + \sum_{p=1}^{2} \lambda_p n_p \qquad \textbf{Equation 8b}$$

where $p$ is the species pertaining only to the products of the reaction. The condition for the minima of the function above at any given point is that the partial derivative of the function with respect to $n_i$ and $\lambda_p$ vanish at this point. An equation solver known as Cantera was used in conjunction with Matlab in order to solve this complex system of equations. Cantera is a software package which performs chemical and thermodynamic equilibrium calculations. It is able to retrieve thermodynamic properties in order to compute equilibrium compositions for mixtures of ideal gases. Thus, this thesis will assume that all gases are considered to be ideal.

## 2.5    Solid Oxide Fuel Cell

### 2.5.1    Fuel Cell Operation

The purpose of the fuel cell [44] is to harness the energy from the syngas produced by the reactor and use it to generate electricity. The amount of electricity produced depends on the efficiency of the fuel cell and the composition of the syngas. Many fuel cell related factors play into the efficiency of the SOFC. One of the factors has to do with reactant transport. If fuel and oxidant are not continually fed to the fuel cell, then the device will ultimately starve. Another factor that directly affects current generated is the speed at which the electrochemical reactions proceed. This is the reason as to why catalysts are often introduced in order to speed up the process. Since ion transport is much more difficult than electron transport, the thinness of the electrolyte also plays a major role in the efficiency of the fuel cell. For this thesis, many of the aforementioned variables will be implemented into the theoretical calculations made in the report by referencing values that have been used in other experiments.

The carbon monoxide and hydrogen from the syngas is fed directly into the anode of the fuel cell to produce the following hydrogen oxidation reaction:

$$CO + H_2 + 2O^{2-} \leftrightarrow H_2O + CO_2 + 2e^-$$
<div align="right">**Equation 9**</div>
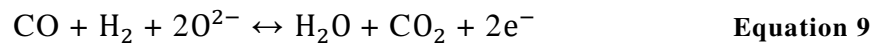
Thus, as opposed to a PEMFC, water is produced at the anode rather than the cathode. As can be seen in **Equation 9**, two electrons are transferred though the circuit for every mole of hydrogen. For every mole of oxygen, 4 electrons would be transferred. Since carbon monoxide is also introduced into the anode, carbon dioxide is also produced with the water. The half-cell reactions occurring at the cathode and anode are mediated by the motion of the oxygen ions shown above. Thus, the oxygen reduction reaction occurring at the cathode is illustrated in **Equation 10**:

$$O_2 + 2e^- \leftrightarrow 2O^{2-}$$
<div align="right">**Equation 10**</div>

Thus, one side of the fuel cell is provisioned with fuel from the reactor while the other side is provisioned with oxidant, in this case air. The amount of $CO$ and $H_2$ will be the determining factor of how much current is produced. To depict this concept, the overall electrochemical equation is shown in **Equation 11**:

$$(1\text{-}x)CO + xH_2 + \tfrac{1}{2}O_2 \leftrightarrow (1\text{-}x)\,CO_2 + xH_2O \qquad x = \frac{n_{H_2}}{n_{mix}}$$
<div align="right">**Equation 11**</div>

where $x$ is the molar fraction of the amount of hydrogen with respect to the mixture. **Figure 2-3** depicts the process and operation of this SOFC:
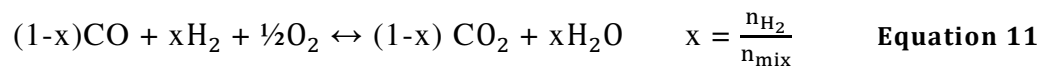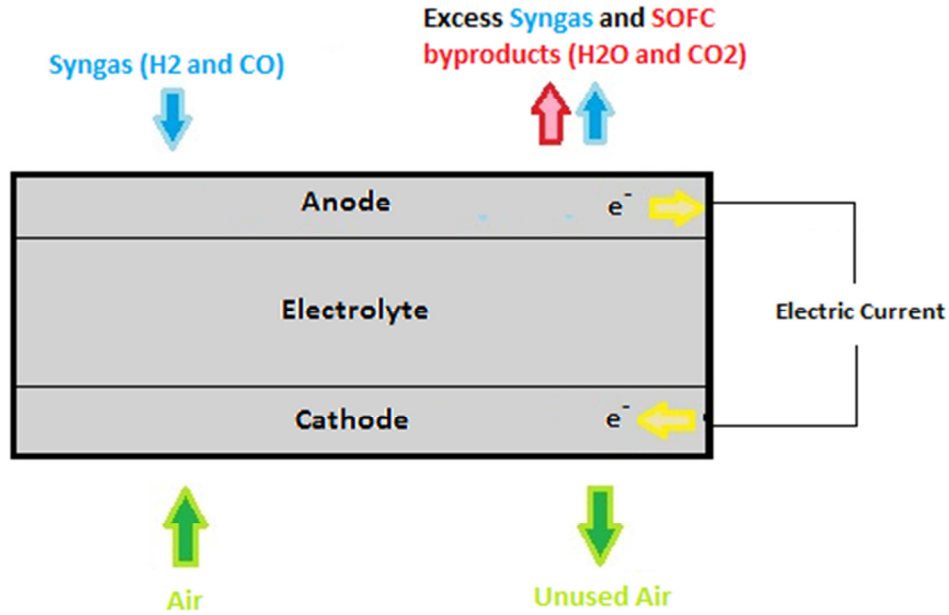
**Figure 2-3:** Overall Diagram of SOFC using Syngas. The carbon monoxide and hydrogen from the syngas of the reactor enter the anode side of the fuel cell to produce a hydrogen oxidation reaction. Two electrons are transferred through the circuit for every mole of hydrogen. Air is provided at the cathode side of the fuel cell in order to ultimately produce water and carbon dioxide with the assistance of ions traveling through the electrolyte membrane.

In order to fully understand the improvements that can be made to fuel cell performance, one must understand that there are irreversible losses that increase with increasing current. In order to calculate the theoretical voltage output, *V*, of a fuel cell, several inputs must be accounted for, as can be seen in **Equation 12**:

$$V = E_{thermo} - \eta_{act} - \eta_{ohmic} - \eta_{conc}$$

**Equation 12**

where $E_{thermo}$ is the thermodynamically predicted reversible fuel cell voltage, $\eta_{act}$ is the activation loss due to reaction kinetics, $\eta_{ohmic}$ is the ohmic loss due to ionic and electronic conduction, and $\eta_{conc}$ is the concentration loss due to mass transport. For this study, the concentration loss will be assumed to be insignificant when compared to the

other losses in the SOFC. This thesis intends on building a simple theoretical thermodynamic model of the SOFC based on values taken from other published papers. Since concentration loss requires too many parameters recorded during actual experimentation, this loss will not be accounted for. At this point, it would be relevant to introduce the role of thermodynamics in this fuel cell process.

## 2.5.2   Thermodynamics

### 2.5.2.1   Gibbs

The fuel cell should be thought of as an open system. Assuming steady state operation, a control volume analysis would show that the fuel cell is allowed to exchange heat with the environment and work would exit as electrical work through the wire connected to the fuel cell. Thus, according to the first law of thermodynamics, heat minus this electrical work is equivalent to the internal energy of the system. The maximum heat energy that is made available by a fuel cell is given as the enthalpy of reaction while the maximum work energy that can be extracted by a fuel cell is given by the Gibbs free energy. Gibbs free energy is the energy needed to create a system and make room for it minus the energy that one can get from the environment due to heat transfer, as shown by the second law of thermodynamics in a reversible process. For the purpose of this thesis, the fuel cell will be assumed to be in an isothermal and isobaric process. This allows for the electrical work to be equal to the negative of the Gibbs free energy difference between the products and the reactants. Since the concentrations of the different species will vary according to the output of the syngas, the Gibbs free energy will be calculated by accounting for the chemical potential, $\mu$, of the system for the different species, $i$, through **Equations 13 and 14**:

$$\mu_i = \mu_i^o + RT\ln a_i \qquad\qquad \textbf{Equation 6}$$

$$dG = \sum_i \mu_i \, dn_i \qquad\qquad \textbf{Equation 7}$$

where $R$ is the universal gas constant, $T$ is the temperature, and $a$ is the activity. Since we are assuming an ideal gas and units of atm for pressure, the activity becomes equivalent to the pressure of the system multiplied by the respective number of moles of a particular species $i$, or $a_i = (n_i)(P)$. Thus, the Gibbs free energy becomes a function of temperature, pressure, and number of moles of a species $i$. The Gibbs free energy for the overall reaction can be calculated through **Equation 15**:

$$\Delta g = \sum_P v_e \Delta g^\circ_e - \sum_R v_i \Delta g^\circ_i + RT\ln \frac{\Pi_e \, a^{v,e}_{product,e}}{\Pi_i \, a^{v,i}_{reactant,i}} \qquad\qquad \textbf{Equation 8}$$

where $\varDelta g^\circ$ is the reference Gibss free energy, $R$ is the universal gas constant, $T$ is the temperature, $v$ represents the number of moles of either an inlet species $i$ or an outlet species $e$. The reference Gibbs free energy can be calculated through **Equation 16:**

$$\Delta g^\circ = \Delta h - T\Delta s \qquad\qquad \textbf{Equation 16}$$

where $h$ is the enthalpy and $s$ is the entropy. As mentioned before, the internal energy of the system is equivalent to the heat minus the work. Assuming negligible kinetic and potential energy, the internal energy becomes equivalent to the change in enthalpy of the system. The second law of thermodynamic simplifies the first law of thermodynamics by making the heat transferred equivalent to the temperature of the system multiplied by the change in entropy of the system.

### 2.5.2.2  Reaction Enthalpy

As mentioned before, the maximum heat that is made available by the fuel cell is given by the enthalpy of reaction of the system.. This is how the fuel cell is able to transfer heat to the reactor. This available energy, or enthalpy of reaction, is the energy needed to create a system plus the work needed to make room for it. The energy needed to create the system, or internal energy, is largely due to the reconfiguration of chemical bonds. For example, the burning of hydrogen bonds releases heat due to molecular bond reconfiguration. As mentioned before, the fuel cell will be assumed to be in an isothermal and isobaric process. In order to calculate the enthalpy of reaction, the formation enthalpies for compounds must first be found. The formation enthalpy is the energy that is released or absorbed when the compound is formed from its stable elements. The formation enthalpies for water, carbon dioxide, and water are all exothermic, thus requiring no heat transfer. The equation used to calculate the reaction enthalpy can be seen in **Equation 17**:

$$\Delta h = \sum_{products}[x_i(h_f + h_T - h_{T = 298\ K})] - \sum_{reactants}[x_i(h_f + h_T - h_{T = 298\ K})]$$

**Equation 17**

where $x$ is the number of moles of species $i$, $h_f$ is the formation enthalpy, $h_T$ is the enthalpy at a given temperature, and $h_{T = 298\ K}$ is the enthalpy at T = 298 K.

### 2.5.3  Reaction Kinetics

The activation loss is associated with the kinetics of the electrochemical reaction occurring within the fuel cell. The rate of the electrochemical reaction directly affects the current generated by the fuel cell. Fuel cell performance is thus enhanced by increasing

the rate of electrochemical reaction. When evaluating the overall rate of reaction, one must consider rates for both the forward and reverse directions of the reaction. The net rate, or the difference between these two directions, along with the exchange current density, $j_o$, allows one to calculate the activation loss, as will be discussed later in this thesis. Normally, the exchange current density is described by **Equation 18**:

$$j_o = nFc_R^*f_1e^{-\Delta G/(RT)} \qquad\qquad \textbf{Equation 18}$$

where $n$ is the number of electrons transferred, $F$ is Faradays constant, $c_R^*$ is the reactant concentration, $f_1$ is the decay rate, and $\Delta G$ is the activation barrier. In order to calculate $\eta_{act}$, many values had to be taken from literature, as will be explained. The main equation used to calculate the activation loss is the Butler-Volmer equation, as can be seen in **Equations 19 and 20**:

$$j = i/A \qquad\qquad \textbf{Equation 19}$$

$$j = j_o(e^{(\alpha nF\eta_{act})/RT} - e^{((1-\alpha)nF\eta_{act})/RT}) \qquad\qquad \textbf{Equation 20}$$

where $\alpha$ is the transfer coefficient, $j$ is the current density, and $j_o$ is the exchange current density. Both the transfer coefficient and exchange current density have been taken from literature due to the fact that they are typically found through experimentation. When implemented into MATLAB, we used the fzero function in order to ensure that only positive values of activation loss with respect to current density were being calculated. These equations, along with assumptions, can be seen in Appendix E.

### 2.5.4   Charge Transport

The ohmic loss can be attributed to the difficulty associated with ion charge transport across the electrolyte and the electron transport across the electrodes. According to Ohm's law, there is a linear relationship between voltage drop and current density. In SOFCs, ionic transport is much more difficult and dominant than electronic charge transport. This is why manufacturers strive to make electrolytes as thin as possible in order to reduce the distance that the ion must travel to get from one electrode to the other. Charge transport has three major driving forces: electrical forces due to electrical potential gradient and conductivity, chemical forces due to chemical potential gradient and diffusivity, and mechanical forces due to pressure gradient and viscosity. Due to the accumulation/depletion of electrons at the two electrodes, a voltage and concentration gradient develops in the electrolyte while only a voltage gradient develops in the electrode. Ohmic loss can be attributed to the fact that fuel cell conductors have resistance, $R_{ohmic}$, to charge flow, thus requiring voltage to provide that extra driving force. This concept can be formulated into **Equation 21**:

$$\eta_{ohmic} = iR_{ohmic} = i(R_{electron} + R_{ion}) = V \qquad \textbf{Equation 21}$$

where *i* is current. As mentioned before, $R_{ion} \gg R_{electron}$. This is due to defects such as vacancies in the crystalline lattice of a typical ionic conductor. Since this thesis focuses more on simple thermodynamic modeling and not material specific properties, we will assume that the voltage gradient is far more dominant than the concentration gradient in the electrolyte. Relevant values will be taken from literature, as can be seen in Appendix F. In order to calculate $\eta_{ohmic}$, the ionic conductivity, $\sigma$, had to be calculated for both the electrode and electrolyte. **Equations 22, 23, and 24** explain how the ohmic loss is calculated:

$$\eta_{ohmic} = j\left(\frac{L_{electrode}}{\sigma_{electrode}} + \frac{L_{electrolyte}}{\sigma_{electrolyte}}\right)$$  **Equation 9**

$$\sigma_{electrode} = \frac{|ze|Fc_e q\tau}{m}$$  **Equation 10**

$$\sigma_{electrolyte} = \frac{c(z_i F)^2 D}{RT}$$  **Equation 11**

where *L* is thickness of the membrane, *z* is amount of charge carried by charged species across the membrane, *c* is the molar concentration of the charge species, *q* is electron charge, $\tau$ is the mean free time between scattering events, *m* is the mass of an electron, and *D* is the diffusivity of the electrolyte. As mentioned before, the concentration loss requires too many parameters recorded during actual experimentation. Also, this paper is mainly focused on the maximum power that can be extracted and the maximum heat that can be made available by the fuel cell. The point on the polarization curve at which these maximums are located occur before the concentration loss region. Thus, this loss will not be accounted for.

### 2.5.5   Literature Review: Internal Reforming SOFC using Syngas

After researching several engineering databases, many papers had been found that did complex research into the area of solid oxide fuel cell using syngas. Many of those papers far exceeded the scope of this thesis, which has more to do with thermodynamic modeling. Thus, we found a paper [45] that consisted mainly of thermodynamic modeling of a solid oxide fuel cell using syngas. The only difference is that the SOFC examined in that paper is directly internal reforming (DIR-SOFC), while the reactor's system examined in this thesis only involves indirect reformation.  The assumptions that are made for this analysis can be seen in the paper itself; this section will serve more as a

summary of operations and results than anything else. The diagram depicting this system can be seen **Figure 2-4**:
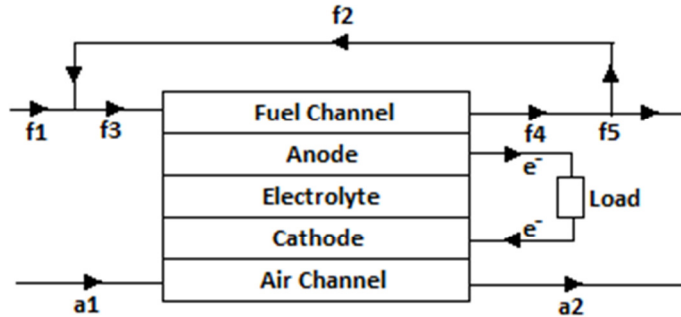


**Figure 2-4**: Overall diagram of DIR-SOFC [45]. Gas mixture with high water content is re-circulated and mixed with syngas before entering the fuel channel.

As can be seen in **Figure 2-4**, several things are happening at the fuel channel. Gas mixture, which has high water content, is re-circulated and mixed with syngas before it enters the fuel channel. In order to get the desired equilibrium molar gas concentrations of $H_2$ and CO, three different reactions occur at the anode: steam reformation of methane, water gas shift reaction, and electrochemical reaction. Since the molar flow rates is known at the inlets shown above, they were able to formulate the equilibrium molar gas concentrations in terms of molar flow rate and the extent of each species in the three electrochemical reactions mentioned above. This thesis also utilizes these variables along with air utilization ratio in order to find the voltage, voltage losses, and efficiency of the model. After modeling their results, it is found that there is a tradeoff between high and low air utilization ratio. A lower air utilization ratio means high mass flow rate of air and lower mass flow rate of fuel, thus increasing the cost of the system and lowering the operating cost of the system. A higher air utilization ratio results in reduction of capital and operating costs of the system, but the system's complexity further increases as opposed to the simplicity of using a lower air utilization ratio. Another observation that is

41

made is that increasing the fuel utilization ratio increased electrical efficiency but decreased power, voltage, air utilization ratio and mass flow rate of fuel. It is thus found that increasing this ratio makes the system thermodynamically stable and economically viable.

# 3  METHODOLOGY

## 3.1  Relevant Thermodynamic Equations

Modeling is performed with the help of MATLAB combined with the Cantera interface in order to allow for ease of computing. Cantera is a suite of software tools for thermodynamic reacting flow problems. In order to calculate $E_{thermo}$, an equation had to be made which effectively calculates the Gibbs free energy, $\Delta g$, with varied temperature $T$, pressure $P$, and molar fraction $x$ of hydrogen entering the anode side of the fuel cell. Based on **Equation 9**, hydrogen and carbon dioxide are the products of the fuel cell operation while oxygen, hydrogen, and carbon monoxide are the reactants. Balancing the overall electrochemical equation, as seen in **Equation 11**, allows us to combine **Equations 11** and **15** in order to calculate the Gibbs free energy of the SOFC. **Equations 25** and **26** explain how reversible fuel cell voltage is calculated:

$$\Delta g = [x(h-(Ts))_{H_2O} + (1-x)(h-Ts)_{CO_2}]_{T,P} - [(1-x)(h-(Ts)_{CO} + \tfrac{1}{2}(h-Ts)_{O_2} + x(h-(Ts))_{H_2}]_{T,P} + RT\ln\frac{1}{\frac{.21P_i}{P^0}} \qquad x = \frac{n_{H_2}}{n_{mix}} \qquad \textbf{Equation 25}$$

$$E_{thermo} = -\frac{\Delta g}{nF}$$

<div align="right">**Equation 26**</div>

where $h$ is enthalpy, $s$ is entropy, $R$ is the universal gas constant, $P_i$ is the partial pressure, and $P^o$ is the standard state pressure, $n$ is the number of electrons transferred, and $F$ is Faraday's constant. Assuming an ideal gas and that all units of pressure are kept in atm, then $P^o$ takes the value of 1 atm. Combing **Equation 17** with **Equation 11**, we were also able to calculate the enthalpy of reaction, as can be seen in **Equation 27**:

$$\Delta h = [x(h_f + h_T - h_{T=298\,K})_{H_2O} + (1\text{-}x)(h_f + h_T - h_{T=298\,K})_{CO_2}] - [(1\text{-}x)(h_f + h_T - h_{T=298\,K})_{CO} - \tfrac{1}{2}(0 + h_T - h_{T=298\,K})_{O_2} - x(0 + h_T - h_{T=298\,K})_{H_2}] \qquad x = \frac{n_{H_2}}{n_{mix}}$$

<div align="right">**Equation 27**</div>

where $h_f$ is the formation enthalpy for unstable elements, $h_T$ is the enthalpy at a given temperature, and $h_{T=298\,K}$ is the enthalpy at T = 298 K. These equations have been implemented into MATLAB, as can be seen in Appendices A and C.

## 3.2 Voltage Losses

As mentioned before, many values for both ohmic and activation loss had to be taken from literature. Since temperature was held constant in the documented papers that were found, the given exchange current density was thus given in terms of that single temperature. Since temperature and current are the only variables for the activation loss of this thesis, all variables that are functions of temperature had to consequently be calculated as a function of temperature. Thus, an expression had to be created in order to calculate the exchange current density with temperature as the only variable. Based on **Equation 18**, the only way to make $j_o$ a function of only $T$ would be to convert every

other variable into a single constant, as can be seen in **Equation 28a**. Consequently, the exchange current density and its respective temperature had to be taken from two different experiments in order to determine an expression based on the aforementioned constants found through mathematical manipulation. This process can be seen in **Equation 28**:

$$j_o = A e^{\frac{-B}{T}}$$  **Equation 28a**

$$j_o = (8.66*10^7) e^{\frac{-22082}{T}}$$  **Equation 28a**

where *A* and *B* are the constants found through mathematical manipulation [44 and 45]. Similar to activation loss, ohmic loss is also only a function of temperature and current for this thesis. Since the diffusivity, *D*, of the electrolyte is a function of temperature, **Equation 24** must account for this change. The diffusivity is given by **Equation 29**, which consequently allows us to calculate the conductivity of the electrolyte through **Equation 30**:

$$D = D_o e^{\frac{-\Delta G}{RT}}$$  **Equation 29**

$$\sigma_{electrolyte} = \frac{D_o c(z_i F)^2 e^{\frac{-\Delta G}{RT}}}{RT}$$  **Equation 30**

where $D_o$ is the constant reflecting the frequency of the hoping process and $\Delta G$ is the activation barrier. **Equation 30** is often simplified into an empirical expression by lumping the varies pre-exponential variables into a single factor, or $A_{SOFC}$. This value, along with $\Delta G$, were taken from literature [44] in order to create an expression defining $\sigma_{electrolyte}$ as a function of only temperature. This expression can be seen in **Equation 31**:

$$\sigma_{\text{electrolyte}} = \frac{A_{\text{SOFC}} e^{\frac{-90,000}{RT}}}{T} \qquad\qquad \textbf{Equation 31}$$

## 3.3  Power Density and Heat

The major inputs to calculate the voltage are temperature, pressure, molar fraction of hydrogen in syngas, and current. Each function was thus called upon from a separate code, which calculated voltage based on these 4 major inputs. The code to calculate voltage can be seen in Appendix G. Once the voltage is found, the power density, $P_d$, can be readily evaluated through **Equation 32**:

$$P_d = V*j \qquad\qquad \textbf{Equation 32}$$

where $V$ is the voltage and $j$ is the current density. The code used to calculate power density can be seen in Appendix H. Once the power density is calculated for each temperature, the maximum power density, or peak power, can readily be found through polynomial fitting in Matlab. Since a fuel cell converts chemical energy into electrical energy, one can calculate the heat dissipated from the fuel cell if the output electrical power and energy input are known. Thus, the heat dissipated from the fuel cell, or $T\Delta s_{fuel\ cell}$, will be subtracted by the heat required by the reactor, or the enthalpy of reaction ($\Delta h_{\text{reactor}}$). This quantity will then be divided by the Gibbs of the fuel cell, or $\Delta G_{fuel\ cell}$, in order to calculate how much energy must be taken away from work and rerouted to heat. This final quantity, or $H'$, can ultimately be seen in **Equation 33**.

$$H' = \frac{\Delta h_{\text{reactor}} - T\Delta s_{\text{fuel cell}}}{\Delta G_{\text{fuel cell}}} \qquad\qquad \textbf{Equation 33}$$

## 4 RESULTS/DISCUSSION
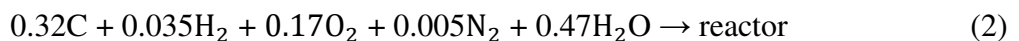
## 4.1 Equilibrium Composition using Cantera

The composition of the syngas entering the fuel cell depends on the operational settings of the reactor, particularly the temperature. For simplicity of calculations, the reactor paper [3] stated as an assumption that pure carbon, or 100% C, is fed into the reactor instead of actual biomass or coal. Thus, these three cases will be analyzed for their potential energy deliverance from the fuel cell. The typical composition of bio-oil, which is created through the pyrolysis process, and coal can be seen in **Table 4-1**:

Table 4-1: Composition of Coal and Biomass

|  | C (%) | O2 (%) | H2 (%) | N2 (%) | S (%) | Ash (%) |
|---|---|---|---|---|---|---|
| **Bio-oil** | 55-64 | 27-40 | 5.1-8 | 0.05-1.0 | 0 | 0.03-6 |
| **Coal** | 65-88 | 7.1-17 | 5.1-6 | 0.9-1.2 | 0.5-5.0 | 9.1-20 |

As can be seen in **Table 4-1**, the hydrogen contents are about the same. However, the carbon content of coal exceeds that of biomass. For this reason, carbon monoxide or carbon dioxide are expected to play a much larger role for coal in the byproduct of the reactor. Coal has a much higher content of ash, which as mentioned before has the potential to create slagging or fouling in the combustor. The biomass has virtually no sulfur, which is a significant contributor to greenhouse gases. A major downside of biomass can be attributed to its relatively higher than normal oxygen content. This

46

ultimately poses a threat to the desirable increase in hydrogen content due to the fact that this hydrogen will potentially bond with the excess oxygen and form much more water than desired. As mentioned before, we used a thermodynamic equilibrium solver called Cantera in order to calculate the theoretical chemical equilibrium composition values of $H_2$, CO, $CO_2$, $CH_4$, and $H_2O$ for pure carbon, coal, and biomass. Cantera uses the element potential method, which is a nonstoichiometric method which involves solving a set of M nonlinear algebraic equations, where M is the number of elements. Cantera finds the composition that minimizes the total Gibbs free energy of the mixture. We held both the temperature and pressure constant for this calculation. We kept the pressure constant at 2 atm. According to the reactor [3], superheated steam is injected with feedstock at 1.5 times the stoichiometric rate of carbon. Thus, the following equations describe the chemical composition of pure carbon (1), biomass (2), and coal (3) going into the reactor:

$$0.4C + 0.6H_2O \rightarrow \text{reactor} \tag{1}$$

$$0.32C + 0.035H_2 + 0.17O_2 + 0.005N_2 + 0.47H_2O \rightarrow \text{reactor} \tag{2}$$

$$0.34C + 0.028H_2 + 0.058O_2 + 0.006S + 0.006N_2 + 0.054Ash + 0.51H_2O \rightarrow \text{reactor} \tag{3}$$

Thus, the significant products of these three different feed-stocks include hydrogen, water, carbon dioxide, carbon monoxide, and methane. These equations were entered into the thermodynamic equilibrium solver in Matlab for different temperatures and implemented into the following graphs, as can be seen in **Figure 4-1**, **Figure 4-2**, and **Figure 4-3**.

**Figure 4-1:** Equilibrium composition of pure carbon as a function of temperature. The molar fraction of the mixture going into the reactor is $0.4C + 0.6H_2O$. Steam-Carbon reaction (Eq. 4) dominates from 400-1000K at a large extent, resulting in increased hydrogen and carbon monoxide content and decreased water and carbon dioxide content. After 1000K, the water gas shift reaction (Eq. 5) shifts toward the reactants to a small extent. These endothermic reactions work against the high hydrogen content, which proves to be unfavorable to the reactor because more air must be used for combustion.
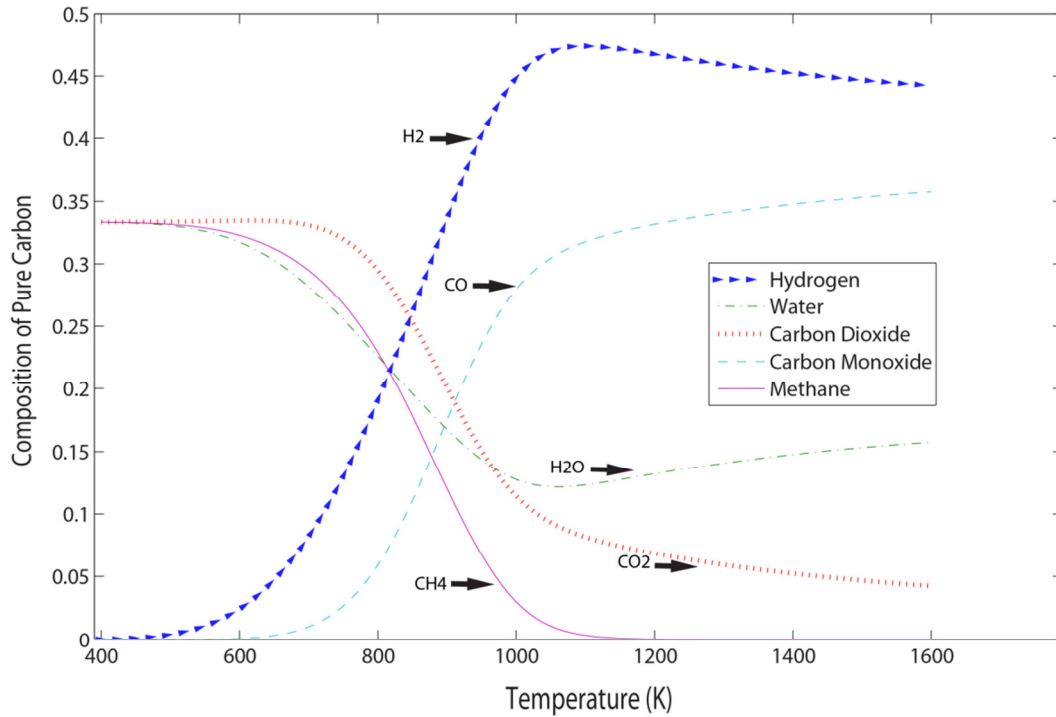
**Figure 4-2:** Equilibrium composition of biomass as a function of temperature.  The molar fraction of the mixture going into the reactor is $0.32C + 0.035H_2 + 0.17O_2 + 0.005N_2 + 0.47H_2O$. From 400-1000K, the Boudouard reaction dominates (Eq. 3). After 1000K, the water gas shift reaction (Eq. 5) shifts toward the reactants as an endothermic reaction. The low hydrogen content is unfavorable for the fuel cell and the endothermic reactions taking place prove to be unfavorable to the reactor because more air must be used for combustion.
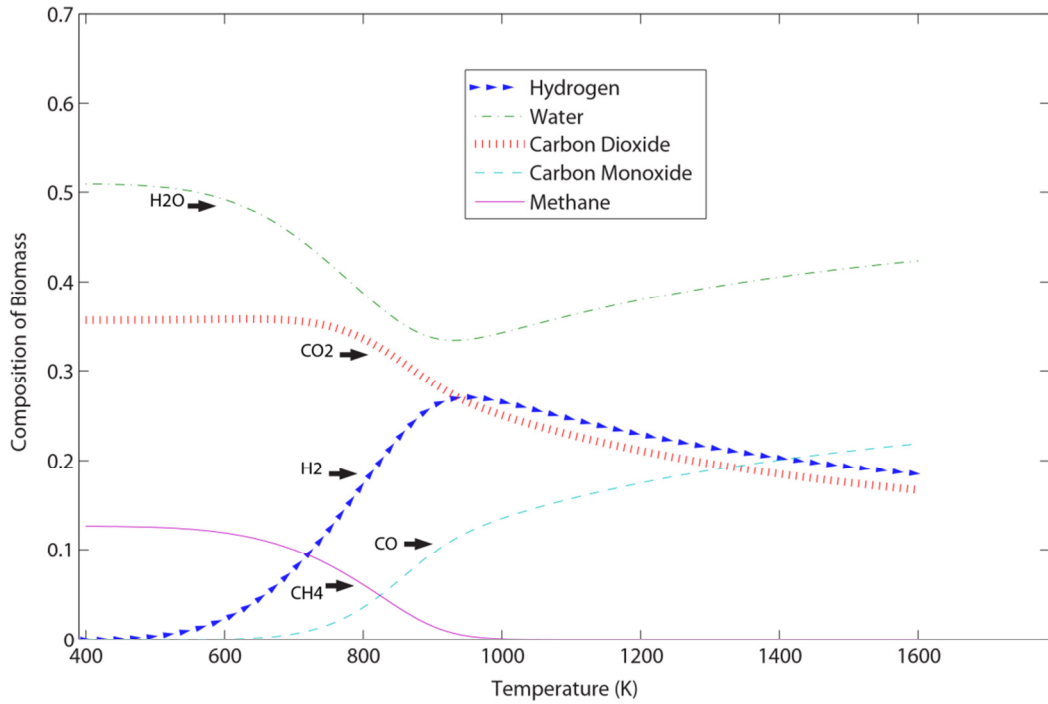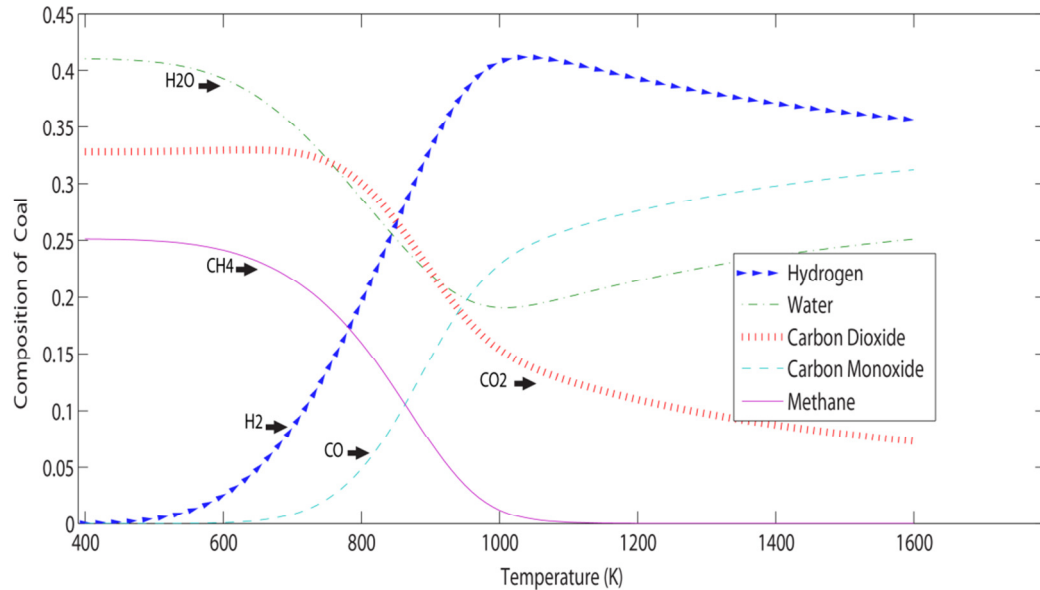
**Figure 4-3:** Equilibrium composition of Coal as a function of Temperature. The molar fraction of the mixture going into the reactor is $0.34C + 0.028H_2 + 0.058O_2 + 0.006S + 0.006N_2 + 0.054Ash + 0.51H_2$. At temperatures below 1000K, the Boudouard (Eq. 3) and steam carbon reaction (Eq. 4) take place as a combined endothermic reaction. Above 1000K, the water gas shift reaction (Eq. 5) shifts towards the reactants, thus being endothermic as well. The high hydrogen content combined with the overall endothermic reaction proves to be favorable for the fuel cell and unfavorable for the reactor.

The optimal concentration of syngas entering the fuel cell would have a higher concentration of hydrogen than anything else in order to ensure that water and carbon dioxide are the only products. The highest concentration that hydrogen is able to achieve for pure carbon is a little under 0.5, as can be seen in **Figure 4-1**. Hydrogen and carbon monoxide increase while water, methane, and carbon dioxide decrease. Since Gibbs free energy is directly related to hydrogen content, an increase in hydrogen content would ultimately result in an increase in the Gibbs free energy. The same trend is seen in **Figure 4-1** for coal. The main difference between the two is that after a temperature of 1000 K, the water is shown to increase at a faster rate for coal over pure carbon, thus causing the hydrogen to decrease at a faster rate as well. It can thus be said that the Boudouard (Eq.

3) and steam carbon reactions (Eq. 4) are causing the carbon dioxide and water levels to decrease while the hydrogen and carbon monoxide increase from temperatures of 400-1000 K. For both coal and pure carbon, the water and carbon monoxide levels are shown to increase after a temperature range of 1000-1200 K while the hydrogen and carbon dioxide decrease. The reason for this is due to the water gas shift reaction (Eq. 5) shifting towards the reactants, as will be explained in **Section 4.1.1**.

**4.1.1  Water Gas Shift Reaction**

As can be seen in the figures of the previous section, hydrogen gradually increases up until about 1100 K. At temperatures exceeding 1100 K, hydrogen composition monotonically decreases while water increases. This phenomenon can be attributed to the water shift reaction occurring in reverse; hydrogen and carbon dioxide are the reactants to products consisting of carbon monoxide and water. The water gas shift reaction is exothermic in the forward reaction (Eq. 5). If the sign of the Gibbs free energy were to transition from positive to negative, the water shift reaction would occur in reverse, making it endothermic. The Gibbs free energy of the water gas shift reaction can be seen in **Figure 4-4**.
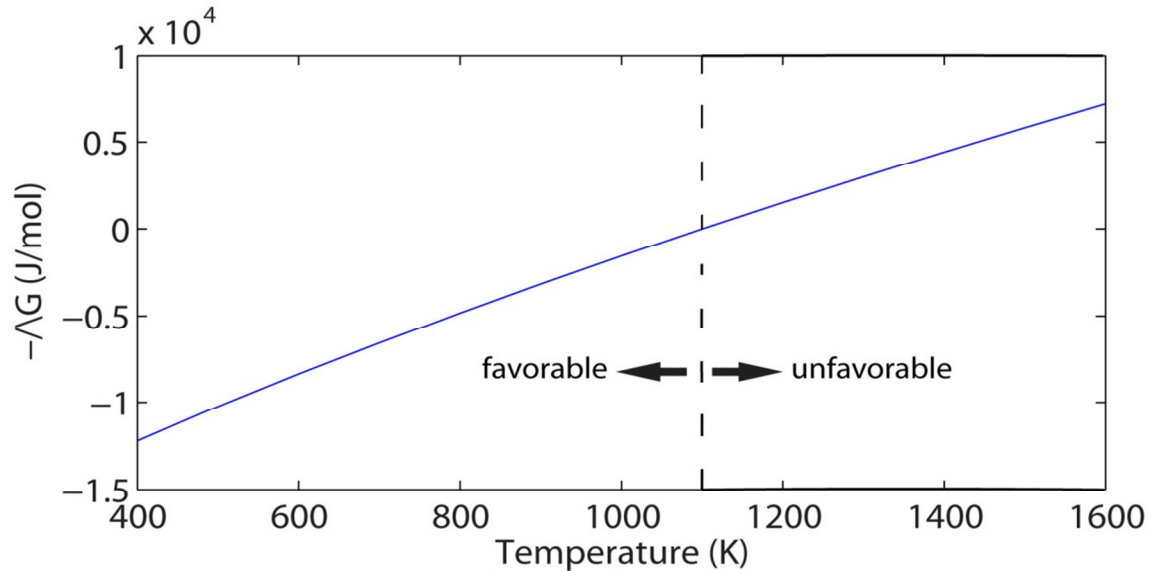
**Figure 4-4:** Gibbs free energy as a function of temperature for the water gas shift reaction. The forward reaction of reactants to products for this reaction is $CO + H_2O \rightarrow CO_2 + H_2$. At temperatures exceeding about 1100K, the reaction occurs in reverse due to the sign change in the Gibbs free energy.

As can be seen in **Figure 4-4**., the water gas shift reaction is thermodynamically unfavorable at higher temperatures. This is illustrated by the continuous decline and eventual sign change in the Gibbs free energy as a function of temperature at around 1100 K. It should be noted that this analysis has been conducted under a modified case in which only CO, $H_2O$, and $CO_2$ are present. The hydrogen performance of biomass is not as favorable as the case for coal, as can be seen in **Figure 4-2**. At temperatures exceeding 1100 K, the water gas shift reaction shifts to the reactants. The compositions for biomass thus shift with increasing temperature less rapidly than pure carbon and coal. The water level is shown to exceed the hydrogen level by as much as 0.2 moles. Although the carbon content and hydrogen content is much less favorable in coal over biomass, as can be seen in **Table 4-1**, the results shown above reflect opposite expected behavior. As will be discussed in section 4.6, fuel oxygen content is a key parameter which impacts the resulting composition and Gibbs free energy. Biomass has much higher oxygen content

than coal, thus increasing the water content at equilibrium. Nonetheless, the composition of coal is shown to have much higher ash content than biomass, thus making it a less clean feedstock option.

## 4.2    Gibbs Free Energy

### 4.2.1    Pure Syngas

Ideally, the only outputs of the reactor would be hydrogen and carbon monoxide, or pure syngas [3]. However, other byproducts, such as water and carbon dioxide, play much larger roles depending on the feedstock being used. This will consequently be analyzed in section 4.2.2. Since the Gibbs free energy of pure syngas is dependent on both composition and temperature, optimal pressure had to be found before coupling the SOFC with the reactor. With pressure constant at 1 atm, we set the temperature to 15 iterations starting at 400 K and ending at 1800 K. We also incremented the hydrogen molar fraction from 0.1 to 0.5 in steps of 0.1. This value of 0.5 can be seen in the equilibrium composition graph as being the highest attainable value of hydrogen content for pure carbon. **Figure 4-5** illustrates a plot showing the Gibbs free energy per mole of the entire mixture as a function of temperature for each molar fraction:
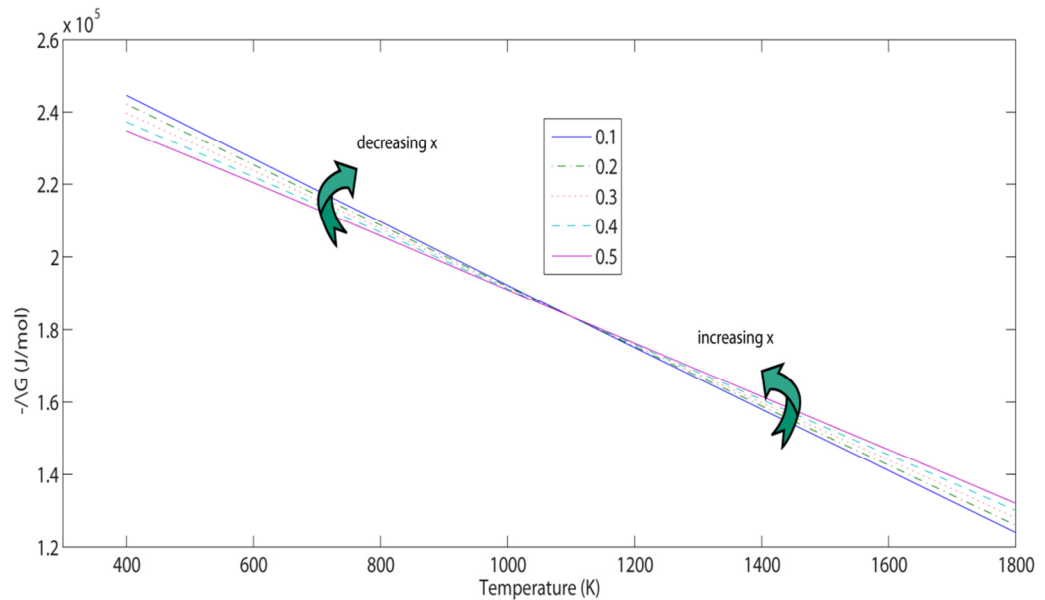
**Figure 4-5:** Gibbs free energy as a function of temperature for each iteration of molar fraction of hydrogen. The electrochemical equation describing the above plot is $(1-x)CO + xH_2 + \frac{1}{2}O_2 \leftrightarrow (1-x)\,CO_2 + xH_2O$, x being the ratio of hydrogen concentration to the entire mixture. For temperatures above 1100 K, the Gibbs free energy is shown to increase as the hydrogen composition increases. For temperatures below 1100 K, the Gibbs free energy is shown to decrease as the hydrogen composition increases. Nonetheless, the Gibbs free energy is much higher at lower temperatures and lower compositions.

As can be seen in **Figure 4-5**, lower temperatures and lower composition levels allowed for a higher Gibbs free energy. However, most SOFCs typically operate at temperatures above 800 K. Thus, the Gibbs free energy is shown to be higher at lower compositions and lower temperatures. This is due to the chemical system having much lower entropy change at lower temperatures than at higher temperatures, thus playing a much larger role in the calculation of free energy of the system. Another noticeable characteristic of **Figure 4-5** is that Gibbs free energy does not increase as the temperature and composition increases until a temperature of 1100 K is reached, which falls in the typical SOFC temperature range.

### 4.2.2　Syngas and Other Reactor Outputs

As can be seen in the composition graphs shown in **Figure 4-1**, **Figure 4-2**, and **Figure 4-3**, pure carbon exhibited the highest hydrogen content while biomass exhibited the lowest hydrogen content of the three cases. The exact opposite can be said about the water content for both cases; biomass exhibited the highest water content. The Gibbs free energy of the reactor was calculated on a per mole oxygen basis for all three cases, as can see seen in **Figure 4-6a**.
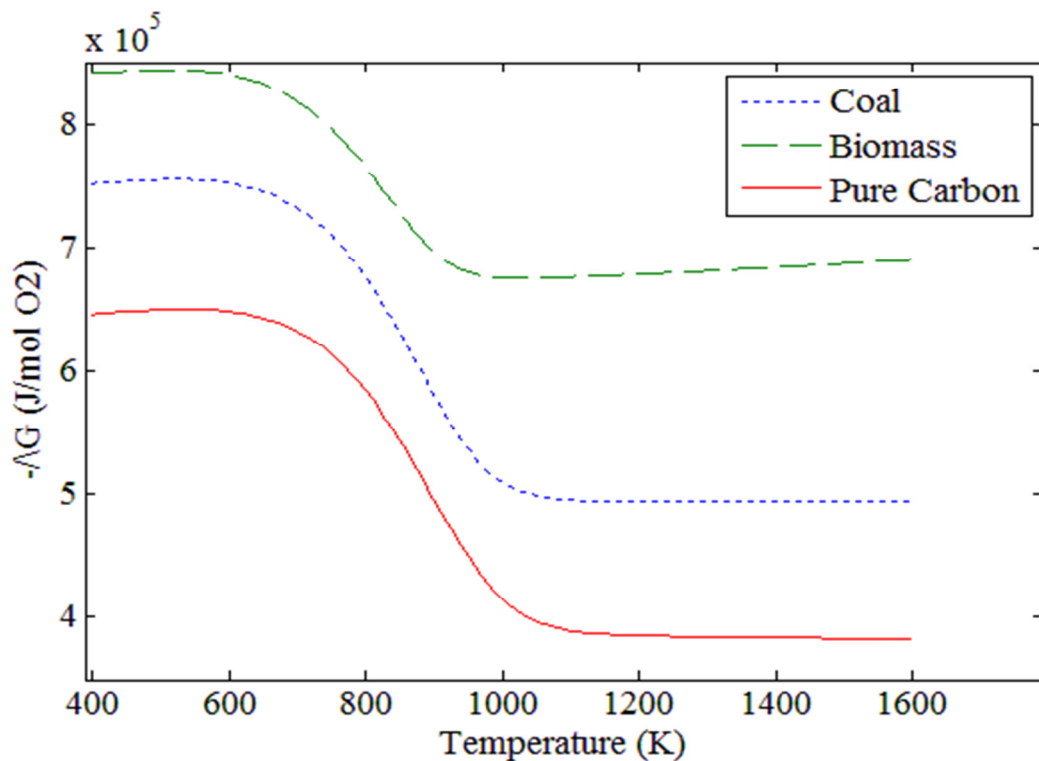


**Figure 4-6a:** Gibbs free energy of the reactor for coal, biomass, and pure carbon. Before 615 K, the Gibbs free energy of the reactant state is shown to be negative; this is shown by the sudden drop in Gibbs free energy for all three cases. Biomass is shown to have a higher value of Gibbs energy, especially after 915 K.

This is due to the product state of the Gibbs free energy for biomass being much higher than the other two cases; the high water content of the biomass-derived syngas is able to compensate for the high water content of biomass going into the reactor. This is not the case for pure carbon and coal. Throughout the prescribed temperature range shown above, the product and reactant state of the Gibbs free energy of coal-derived syngas was shown to have higher values than pure carbon-derived syngas. After 915 K, the reactant state of the Gibbs free energy was shown to be higher for pure carbon over coal. This ultimately gave coal a higher magnitude in Gibbs free energy over pure carbon.

As can be seen in **Figure 4-6a**, biomass-derived syngas is shown to exhibit the highest Gibbs free energy while pure carbon exhibits the lowest Gibbs free energy. In order to attain more work from a fuel cell, the Gibbs free energy of the product state of the reaction must be increased or the Gibbs free energy of the reactant state must be decreased in order to achieve a high magnitude. Based on **Figure 4-6a**, the Gibbs free energy of the product of the fuel cell must compensate for the high energy given off from biomass-derived syngas. As mentioned before, the fuel cell must also compensate for the heat required for reaction in the reactor, or the change in enthalpy. The enthalpy of reaction of the reactor was calculated on a per mole oxygen basis for all three cases, as can see seen in **Figure 4-6b**.
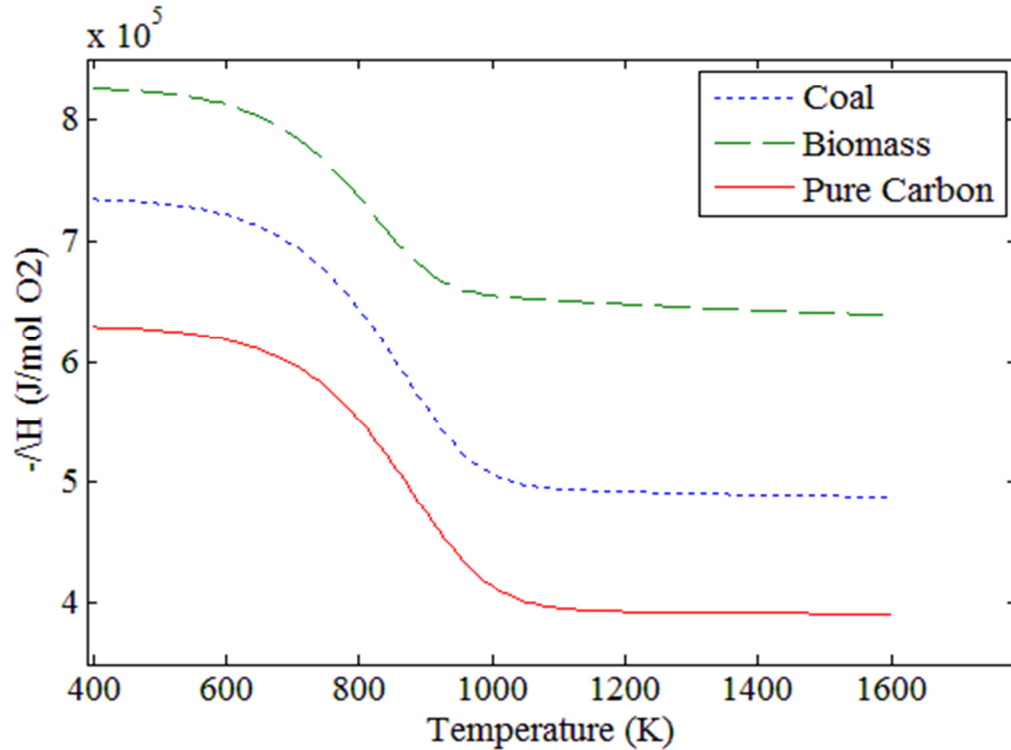
**Figure 4-6b:** Enthalpy of reaction of the reactor for coal, biomass, and pure carbon. Before 610 K, the enthalpy of the reactant state is shown to be negative; this is shown by the sudden drop in Gibbs free energy for all three cases. Biomass is shown to have a higher value of enthalpy change, especially after 915 K. This is due to the enthalpy of the product state for biomass being much higher than the other two cases. Thus, more heat is required for the biomass-based reaction over the other two cases. Throughout the prescribed temperature range shown above, the change in enthalpy of coal-derived syngas was shown to have higher values than pure carbon-derived syngas. After 915 K, the enthalpy of the reactant state was shown to be higher for pure carbon over coal. This ultimately gave coal a higher magnitude in change in enthalpy over pure carbon.

As can be seen in **Figure 4-6b**, biomass-derived syngas is shown to exhibit the highest change in enthalpy while pure carbon exhibits the lowest change in enthalpy. In order for the reaction in the reactor to require less heat, the enthalpy of the product state of the reaction must be decreased or the enthalpy of the reactant state must be increased in order

to achieve a lower change in enthalpy. Based on **Figure 4-6b**, the fuel cell will have to release more heat to compensate for the high change in enthalpy of the biomass-derived syngas.

In order to clearly see how the results of **Figure 4-6a** affected the fuel cell, we calculated the Gibbs free energy for each case. We calculated the Gibbs free energy for the fuel cell by extracting the molar fractions, $x_i$, for each temperature for all three cases and implementing them into **Equation 34**:

$$x_{H2}\ H2 + x_{CO}CO + x_{H2O}\ H2O\ +\ x_{CO2}\ CO2 + x_{CH4}\ CH4 + x_{O2}\ O2\ \rightarrow\ x2_{CO2}\ CO2 + x2_{H2O}\ H2O \qquad \textbf{Equation 34}$$
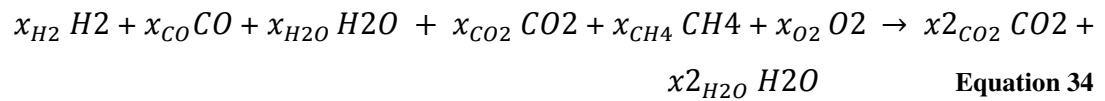
Thus, we assumed that the only products of the overall electrochemical reaction in the fuel cell would be carbon dioxide and water in order to calculate the stoichiometric amount of oxygen. We applied stoichiometry in order to balance the above equation and consequently find the molar fraction of the unknowns: $x_{O2}$, $x_{CO2}$, and $x_{H2O}$. **Equations 35, 36, and 37** describe how the unknown molar fractions are functions of the known molar fractions:

$$x2_{CO2} = x_{CO} + x_{CO2} + x_{CH4} \qquad \textbf{Equation 35}$$

$$x2_{H2O} = \frac{(2*x_{H2})\ +(2*x_{H2O})\ +(4*x_{CH4})}{2} \qquad \textbf{Equation 36}$$

$$x_{O2} = \frac{(2*x2_{CO2})\ +\ x2_{H2O} - x_{CO} - x_{H2O}\ -(2*x_{CO2})}{2} \qquad \textbf{Equation 37}$$

Once we solved for the unknowns, we then proceeded to calculate the Gibbs free energy in terms of the oxygen used at the cathode side of the fuel cell. This consequently allowed us to see the effect of the stoichiometric amount of oxygen on the Gibbs free energy of the fuel cell with water and carbon dioxide as the only outputs. In order to confirm that water and carbon dioxide were the only significant products of the fuel cell in terms of amount, we inputted all the molar fractions of the reactants, including the stoichiometric amount of oxygen, into the thermodynamic equilibrium solver in Matlab. Like before in section 2.5.2.1, we varied the Gibbs free energy, $\Delta$g, with respect to temperature (T) and molar fractions of hydrogen, water, carbon dioxide, carbon monoxide, and methane entering the anode side of the fuel cell. Like before, we kept the pressure atmospheric. **Equation 38,** with the assistance of **Equation 15,** explains how we calculated the Gibbs free energy of the fuel cell:

$$\Delta g = \sum_P v_e \Delta g^\circ_e - \sum_R v_i \Delta g^\circ_i + RT \ln \frac{\prod_e a^{v,e}_{product,e}}{\prod_i a^{v,i}_{reactant,i}}$$

$$\sum_P v_e \Delta g^\circ_e = [x2_{H2O}(\text{h-Ts})_{H_2O} + x2_{CO2}(\text{h-Ts})_{CO2}]_{T,P} \qquad \textbf{Equation 38a}$$

$$\sum_R v_i \Delta g^\circ_i = [x_{CO2}(\text{h} - \text{Ts})_{CO2} + x_{CH4}(\text{h} - \text{Ts})_{CH4} + x_{H2O}(\text{h} - \text{Ts})_{H_2O} + x_{CO}(\text{h-Ts})_{CO}$$
$$+ x_{O2}(\text{h-Ts})_{O_2} + x_{H2}(\text{h-Ts})_{H_2}]_{T,P} \qquad \textbf{Equation 38b}$$

Due to the increase in reactants and products, the activities play a larger role than they did for the case of pure syngas in **Equation 25**, as can be seen in Appendix B. The Gibbs free energy in terms of moles of oxygen can be seen **Figure 4-6c**.
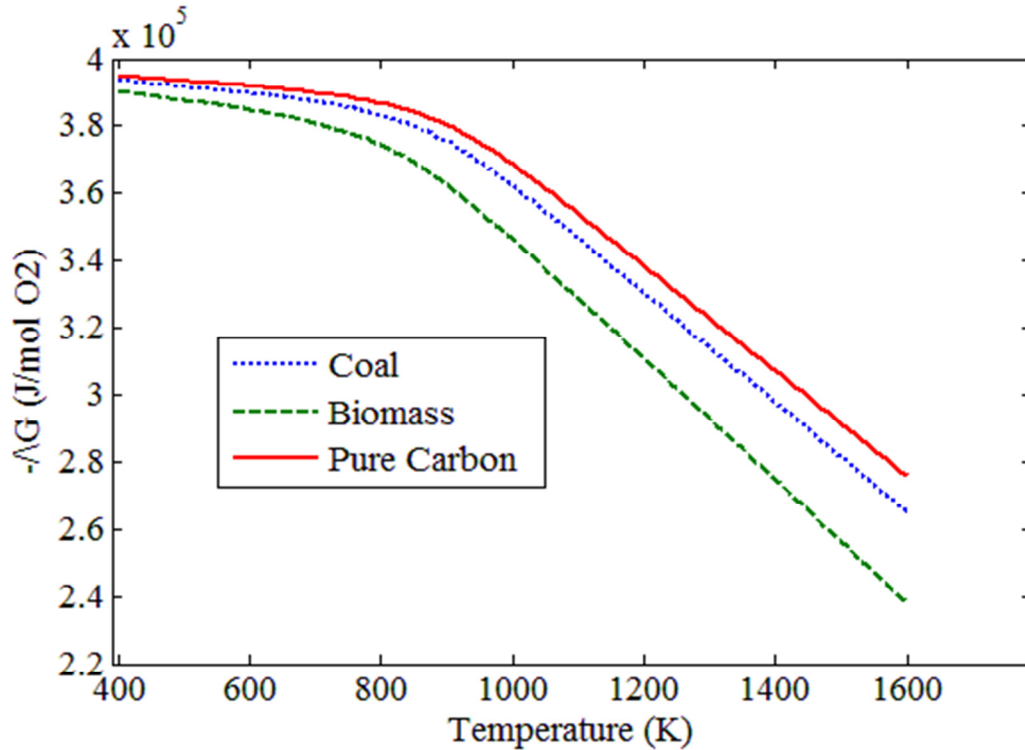
**Figure 4-6c:** Gibbs free energy per mole oxygen as a function of temperature of the fuel cell for biomass, coal, and pure carbon. We assumed carbon dioxide and water to be the only outputs with carbon dioxide, water, carbon monoxide, methane, and hydrogen as the only inputs. We found the Gibbs free energy after calculating the stoichiometric amount of oxygen needed to balance the chemical equation with the aforementioned inputs and outputs. Biomass had the lowest performance while pure carbon exhibited the highest performance. High oxygen content in the biomass resulted in more water and less hydrogen in the reactor output. This high oxygen content hindered the performance of the biomass because it results in a lower heating value for the syngas, this directly affecting the performance of the Gibbs curve. Pure carbon had the highest performance because it was oxygen-free before the reactor and hydrogen-rich after the reactor, as can be seen in **Figure 4-1**.

As can be seen in **Figure 4-6c**, all of the profiles assume similar behavior; Gibbs free energy decreases as temperature increases. Based on the composition graphs in the previous section, we observed that the final product of the reactor based on biomass feedstock had lower hydrogen content than pure carbon and coal. This is consequently reflected in **Figure 4-6c**. However, low hydrogen content was not the only variable that

60

hindered the performance of biomass feedstock. Biomass had the largest content of oxygen compared to the other two feedstocks. For this reason, carbon monoxide and water content exceeded hydrogen content as we increased the temperature in the reactor. This high oxygen content in biomass often results in a low heating value for the product syngas, thus minimizing the potential for a higher Gibbs free energy. This high oxygen content also leads to production of volatile matter and high moisture content, which can be detrimental to the combustion process in the gasifier. Thus, it is not uncommon for gasifiers to incorporate deoxygenation into their design in order to lower the oxygen content of the fuel. The most common deoxygenation technologies are hydrodeoxygenation and hydrocracking [47], which uses 66 kg of hydrogen per metric ton of biomass. Thus, as more hydrogen is used to deoxygenize the biomass, the long term sustainability of the fuel becomes less promising. Many different mechanisms involving catalysts for deoxygenation have been researched and documented; very few have actually been prototyped. The effect of oxygen on fuel cell performance is further explained in 4.6.

## 4.3    Combined Polarization Curves

Once the voltage losses for the fuel cell had been found, we proceeded to calculate the real output voltage. In order to get a better understanding of how this voltage would change as a function of temperature, we plotted 4 distinct polarization curves in Matlab for temperatures ranging from 1000-1400 K. We assumed the molar fraction of hydrogen to be 0.5, which is the highest attainable value found in Section 4.1. We also assumed the pressure to be atmospheric. The polarization curves for pure syngas, biomass, coal, and pure carbon can be seen in **Figure 4-7**, **Figure 4-7**, **Figure 4-7**, and **Figure 4-7**, respectively.

**Figure 4-7:** Polarization curves for pure syngas for temperatures exceeding 1000K. The reversible cell voltage decreases from .99 V at 1000 K to .83 V at 1400 K. As temperature increases, activation loss and ohmic loss decrease, thus making the curve less steep.
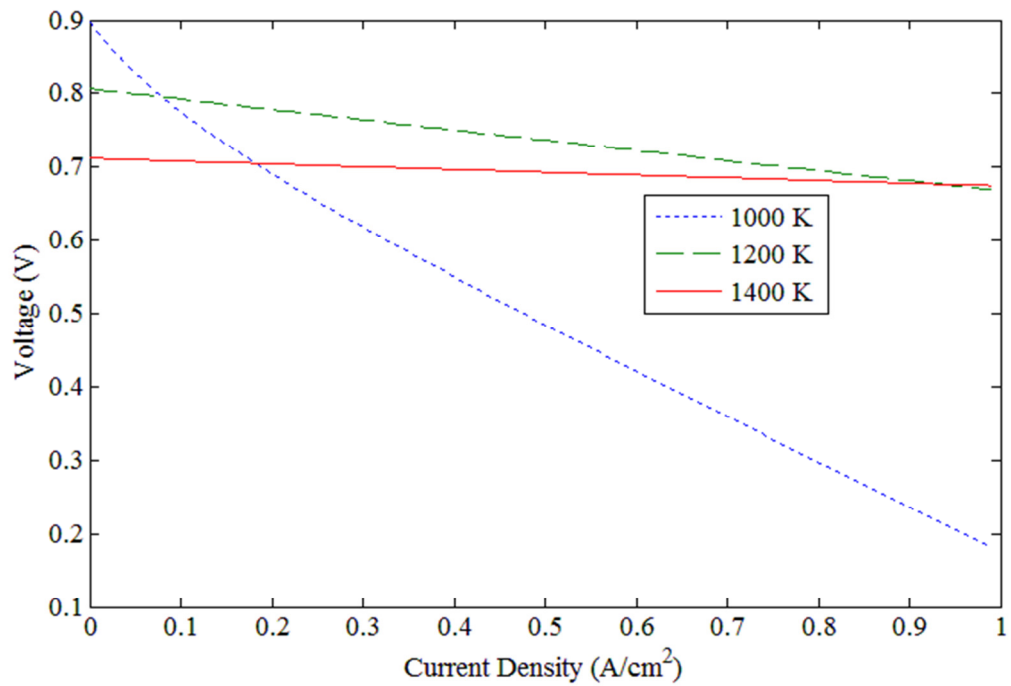
**Figure 4-8:** Polarization curves for biomass-derived syngas for temperatures exceeding 1000K. The reversible cell voltage decreases from .90 V at 1000 K to .71 V at 1400 K. As temperature increases, activation loss and ohmic loss decrease, thus making the curve less steep.
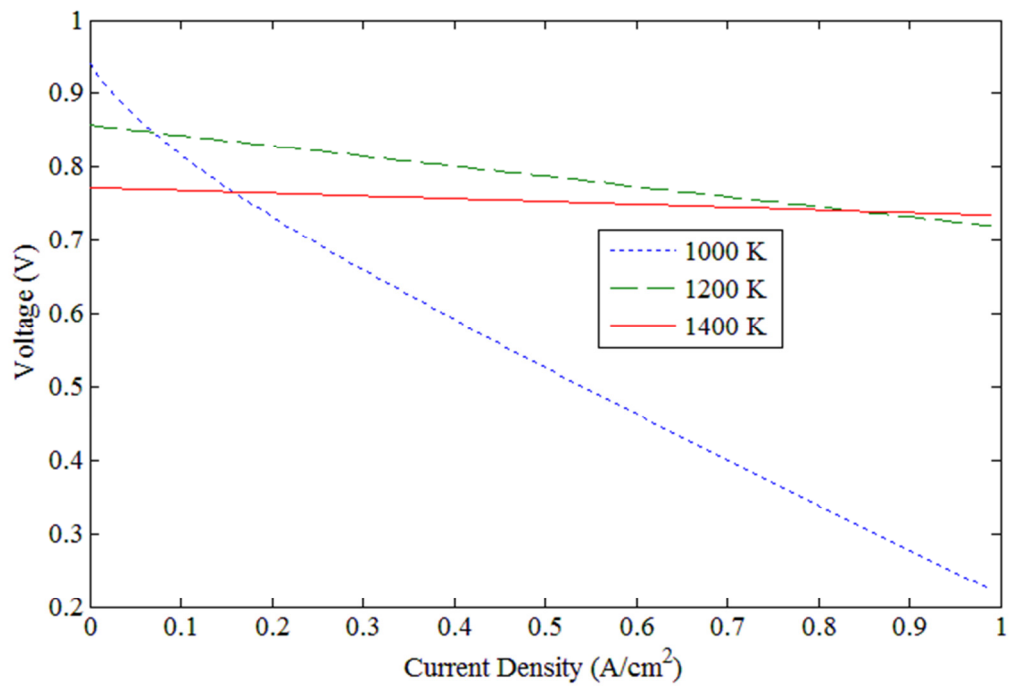
**Figure 4-9:** Polarization curves for coal-derived syngas for temperatures exceeding 1000K. The reversible cell voltage decreases from .94 V at 1000 K to .77 V at 1400 K. As temperature increases, activation loss and ohmic loss decrease, thus making the curve less steep.
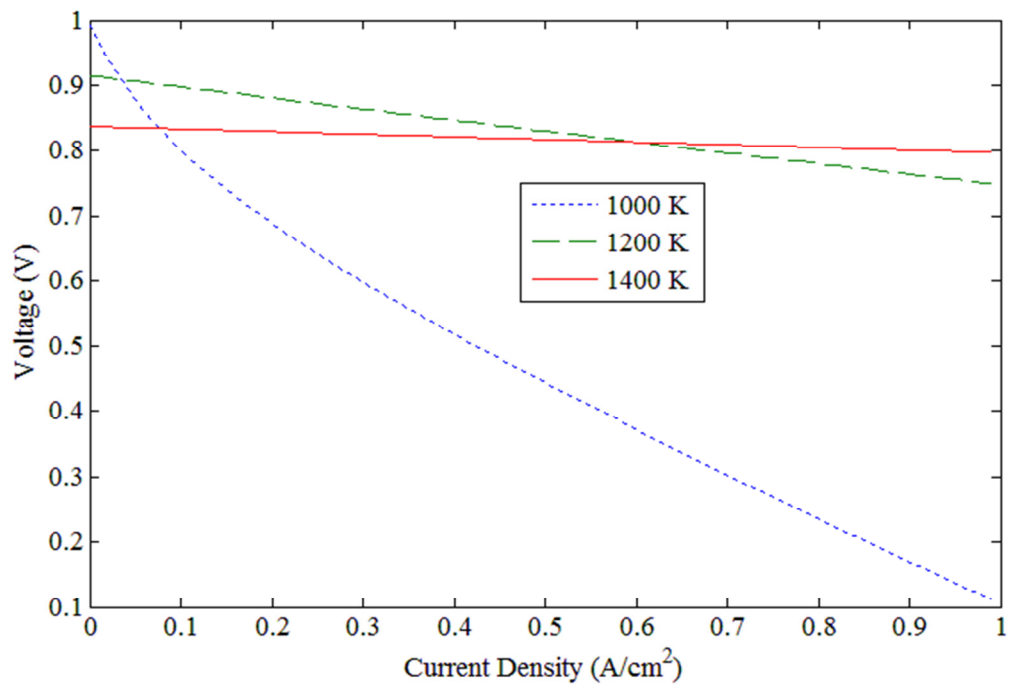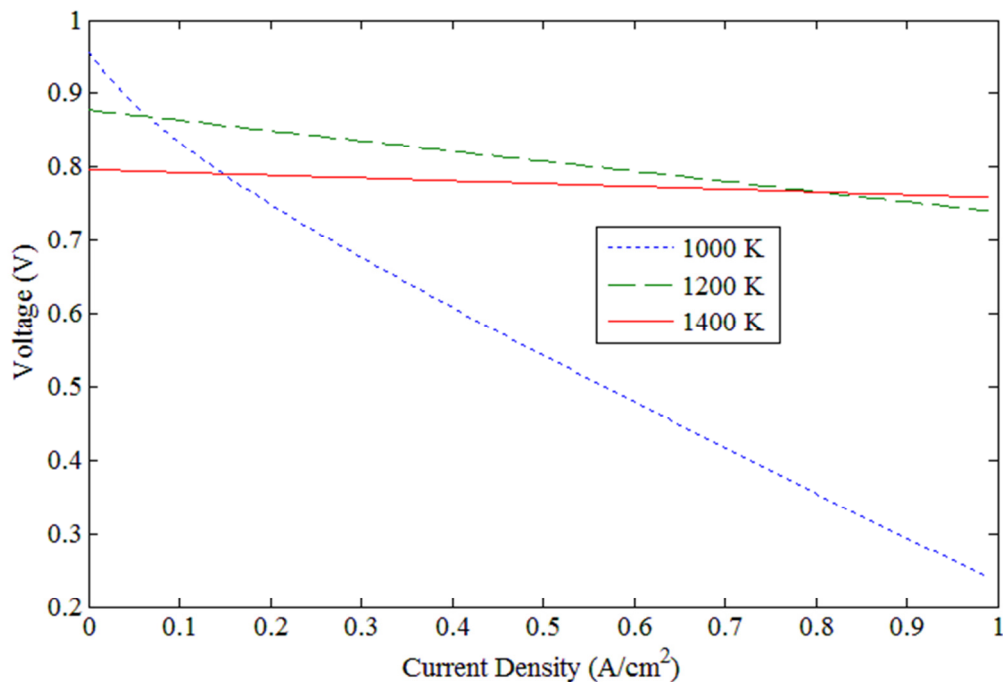
**Figure 4-10:** Polarization curves for pure carbon-derived syngas for temperatures exceeding 1000K. The reversible cell voltage decreases from .95 V at 1000 K to .80 V at 1400 K. As temperature increases, activation loss and ohmic loss decrease, thus making the curve less steep.

As can be seen in **Figure 4-7**, **Figure 4-7**, **Figure 4-7**, and **Figure 4-7**, pure syngas has the highest voltage, followed by pure carbon, coal, and finally biomass. The reversible cell voltage gradually decreases as the temperature increases. The trend can be seen in the figures above. For example, in **Figure 4-7**, the reversible cell voltage is about 0.99 V for T = 1000 K, yet its value drops down to 0.83 V for T = 1400 K. Further observation had shown that the range for optimal current density for maximum power had also increased as temperature increased. In **Figure 4-7**, for example, the current density range increases from 2.54 $\frac{A}{cm^2}$ at 1000 K to 2.87 $\frac{A}{cm^2}$ at 1200 K, which is not shown in the figure. The current density then steadily decreases to 2.3 $\frac{A}{cm^2}$ at 1400 K. This inherently affects the

behavior of the curve for each temperature; as the temperature increases, the curve becomes less steep. This is due to the ohmic and activation losses decreasing as temperature increases. The ohmic loss dominates the activation loss, which is very minimal at this point. Nonetheless, as the temperature increases, both the ohmic and activation losses as a function of current density become linear. This linear behavior consequently affects the polarization curve, as can be seen in the figures above.

## 4.4    Maximum Power Density

### 4.4.1    Pure Syngas

In order to find the maximum power point, or MPP, for a specified setting of the fuel cell, a polynomial curve fit had to be applied to each power density curve. After we fitted the curve, we calculated the derivative of that polynomial in order to find the maxima of the original power density curve. **Figure 4-11** illustrates the MPP as a function of temperature. We kept the composition and pressure constant at x = 0.5 and P = 1 atm.
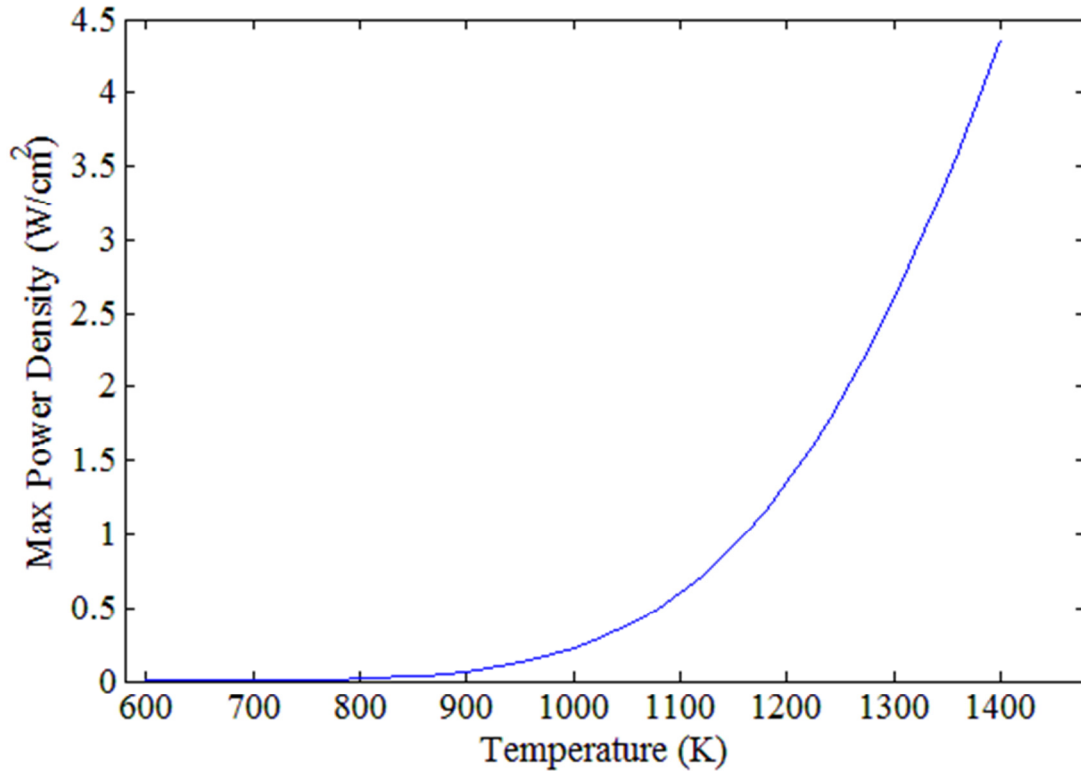
**Figure 4-11:** Maximum power density as a function of temperature of pure syngas. We calculated the power densities for each temperature by multiplying the voltage for a given temperature shown in **Figure 4-7** by its respective current density. We then applied a polynomial curve fit to the power density curve for each temperature. The roots of these polynomials gave us the maximum power density for each temperature. The MPP gradually increases from 600-1400 K. The current density at which these maximum power densities occur increases as the temperature increases.

As can be seen in **Figure 4-11**, the power density gradually increases from 600-1400 K. The maximum power density is shown to be about 4.4 $\frac{W}{cm^2}$ at 1400 K. Between 600 and 800 K, the MPP is nearly zero. Thus, it can be said the MPP increases as the temperature increases. This is due to the insignificant ohmic and activation losses at higher temperatures. However, the MPP at higher temperature requires a much wider range of current density. For example, the MPP occurs at a current of .5644 $\frac{A}{cm^2}$ at 1000 K and at a

current of $10.4334 \frac{A}{cm^2}$ at 1400 K. Thus, higher MPP can be achieved at higher temperatures at the expense of using more current density. However, SOFCs do not typically operate at temperatures as high as 1400 K. As mentioned before, SOFCs generally operate at temperatures between 775 – 1275 K. Nonetheless, if the SOFC is operated at very high temperatures, then the high current density shown from the results above indicates that the concentration loss must be accounted for in order to properly calculate the maximum power of the fuel cell.

### 4.4.2  Syngas and Other Reactor Outputs

The main goal of this project is to observe how well realistic values match up with the ideal case of syngas consisting of only hydrogen and carbon monoxide. Realistically, the output product of the reactor would consist of hydrogen, carbon monoxide, carbon dioxide, methane, and water. Thus, through implementation of the Gibbs free energy data shown in the previous section into a pre-written voltage code, we were able to calculate the maximum power point as a function of temperature. The results can be seen in **Figure 4-12**.
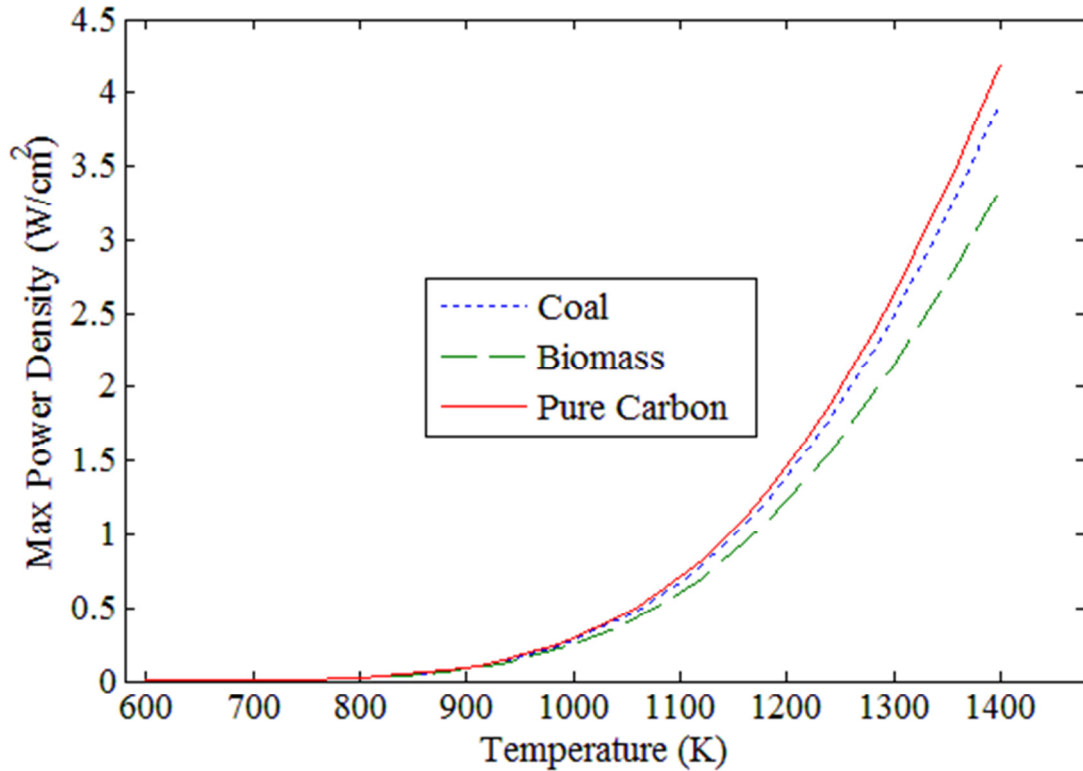
**Figure 4-12:** Maximum power density as a function of temperature or biomass, coal, and pure carbon. We calculated the power densities for each temperature by multiplying the voltage for a given temperature by its respective current density. We then applied a polynomial fit to the power density curve for each temperature. The roots of these polynomials gave us the maximum power density for each temperature. The MPP gradually increases from 600-1400 K, finally reaching a value of about 4.188 $\frac{W}{cm^2}$ for pure carbon, 3.937 $\frac{W}{cm^2}$ for coal, and 3.346 $\frac{W}{cm^2}$ for biomass at 1400 K. The current density at which these maximum power densities occur increases as the temperature increases.

**Figure 4-12** closely exhibits similar asymptotic behavior as **Figure 4-11**. The MPP gradually increases as temperature increases. The MPP is shown to be about 4.188 $\frac{W}{cm^2}$ for pure carbon, 3.937 $\frac{W}{cm^2}$ for coal, and 3.346 $\frac{W}{cm^2}$ for biomass at 1400 K. Just like in **Figure 4-11**, the current density at which these MPP's occur increases as the temperature increases as well. According to **Figure 4-12**, pure carbon exhibits the highest MPP for

any given temperature, following by coal and biomass. However, what is not shown on the figure above is that the current density for pure carbon at any given temperature is larger than that of coal and biomass. For example, at 1400 K, the MPP occurs at 10.53 $\frac{A}{cm^2}$, 10.21 $\frac{A}{cm^2}$, and 9.41 $\frac{A}{cm^2}$ for pure carbon, coal, and biomass, respectively. Thus, just as in **Figure 4-11**, higher MPP can be achieved at higher temperatures at the expense of using more current density. At these higher and impractical temperatures, however, concentration loss would have to be accounted for. As mentioned before, the thermodynamic model shown in this thesis does not account for concentration loss.

## 4.5    Heat Dissipation

In order to calculate the amount of heat being dissipated from the fuel cell, we inputted the reactants and products for biomass, coal, and pure carbon into **Equation 16** for a temperature range of 400-1600 K in order to solve for the entropy; by subtracting the enthalpy of reaction from the Gibbs free energy of the fuel cell, the heat released, $T\Delta s_{fuel\ cell}$, was thereby calculated. We then calculated the enthalpy of reaction for the reactor, $\Delta H_{rxn,reactor}$, (Eq. 17) through the thermodynamic solver in Matlab's Cantera. The code used to calculate this value can be seen in Appendix D. After we found the enthalpy of reaction for the reactor, we then implemented **Equation 33** into Matlab in order to observe how temperature effected the heat dissipation. This equation is reiterated for clarification:

$$H' = \frac{\Delta H_{rxn,reactor} - T\Delta s_{fuel\ cell}}{\Delta G_{fuel\ cell}} \qquad \textbf{Equation 33}$$

If *H'* is closer to 1, then insufficient heat is being supplied to the reactor and energy must be taken away from the work the fuel cell performs, or Gibbs free energy, in order to

provide heat to the reactor. If $H' \ll 1$, then the fuel cell is releasing sufficient heat; less oxygen has to be combusted in order to heat the steam which drives the endothermic reactions in the reactor. Since pure carbon's elemental composition does not contain oxygen, $H'$ was calculated on a per mol $H_2O$ basis for all three cases The results of this analysis can be seen in **Figure 4-13** in terms of mole oxygen produced at the cathode side of the fuel cell.
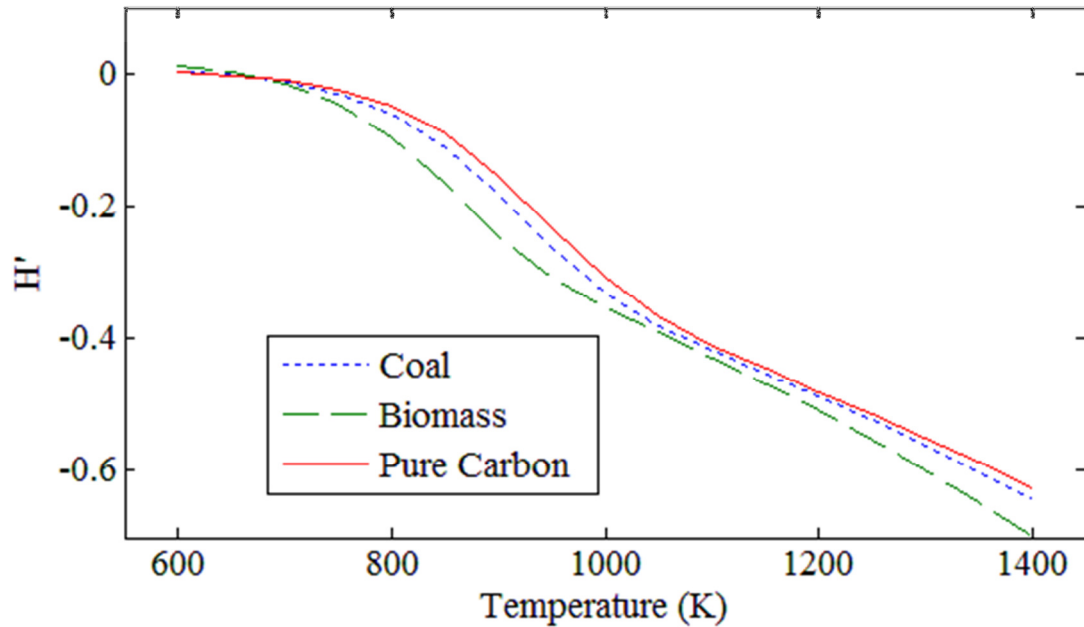


**Figure 4-13:** Ratio of heat dissipated from fuel cell subtracted from enthalpy of reaction of reactor to Gibbs free energy of fuel cell as a function of temperature for Biomass, Coal, and Pure carbon. This ratio, or H', is shown to be higher for Pure Carbon over Coal and Biomass. H' steadily becomes more negative as temperature increases; this ultimately means that the enthalpy of reaction of the reactor is decreasing while the heat released from the fuel cell is increasing as a function of temperature. Pure carbon has the lowest magnitude of $\Delta H_{rxn,reactor}$ and the highest magnitude of $T\Delta s_{fuel\ cell}$ at each temperature, making it the best option for heat dissipation.

As can be seen in **Figure 4-13**, the *H'* value for biomass and coal are lower than pure carbon, with biomass having the lowest H' value for the prescribed temperature range. The key outcome of the figure above is that for all three cases, heat transferred to the environment by the fuel cell exceeds that required for the endothermic reaction in the reactor. The magnitude of $\Delta H_{rxn,reactor}$ steadily decreases as temperature increases for all three cases, with pure carbon having the lowest $\Delta H_{rxn,reactor}$ value and biomass having the highest $\Delta H_{rxn,reactor}$ value at each temperature. The magnitude of $T\Delta s_{fuel\ cell}$ increases as temperature increases for all three cases, with biomass having the lowest $T\Delta s_{fuel\ cell}$ value and pure carbon having the highest $T\Delta s_{fuel\ cell}$ value at each temperature. Thus, this shows that pure carbon is the overall best option out of the three cases: it produces more power and more heat than biomass and coal. The case for coal exhibited a higher *H'* value than that of biomass. This is possibly due to the biomass producing more water at the cathode side of the fuel cell than coal. As seen in **Figure 4-2**, the composition of biomass-derived syngas attained higher values in water content than coal and pure carbon. The use of coal would give overall better performance at the cost of more ash and more burning of oxygen. The use of biomass would require less burning of oxygen and release less ash at the cost of lower work performance and lower heat deliverance.

## 4.6  Biomass Deoxygenation

As mentioned before, biomass has the lowest performance compared to pure carbon and coal due its higher oxygen content. To illustrate this idea more clearly, the Gibbs free energy was calculated for two different molecular amounts of oxygen content in biomass. We then compared this curve to the original molecular amount of oxygen content in biomass shown in section 4.1. The composition of biomass before and after the

injection of steam in the reactor for each case, including the case used in prior analysis, can be seen in **Table 4-2**.

Table 4-2: Variation of oxygen content in Biomass

| Biomass w/ .15 $O_2$ | | C | H2 | O2 | N2 | Ash | H2O |
|---|---|---|---|---|---|---|---|
| | Before Steam Injection | 0.6 | 0.07 | 0.15 | 0.01 | 0.01 | - |
| | After Steam Injection | 0.34 | 0.04 | 0.09 | 0.006 | 0.006 | 0.52 |
| Biomass w/ .32 $O_2$ | | | | | | | |
| | Before Steam Injection | 0.6 | 0.7 | 0.32 | 0.01 | 0.01 | - |
| | After Steam Injection | 0.32 | 0.036 | 0.17 | 0.005 | 0.005 | 0.47 |
| Biomass w/ .45 $O_2$ | | | | | | | |
| | Before Steam Injection | 0.6 | 0.7 | 0.45 | 0.01 | 0.01 | - |
| | After Steam Injection | 0.3 | 0.034 | 0.22 | 0.005 | 0.005 | 0.44 |

The biomass configuration used in Section 4.1 is shown in **Table 4-2** as "Biomass w/ .32 $O_2$". We then proceeded to calculate the Gibbs free energy for each of these cases. The results of this analysis can be seen in **Figure 4-14**.
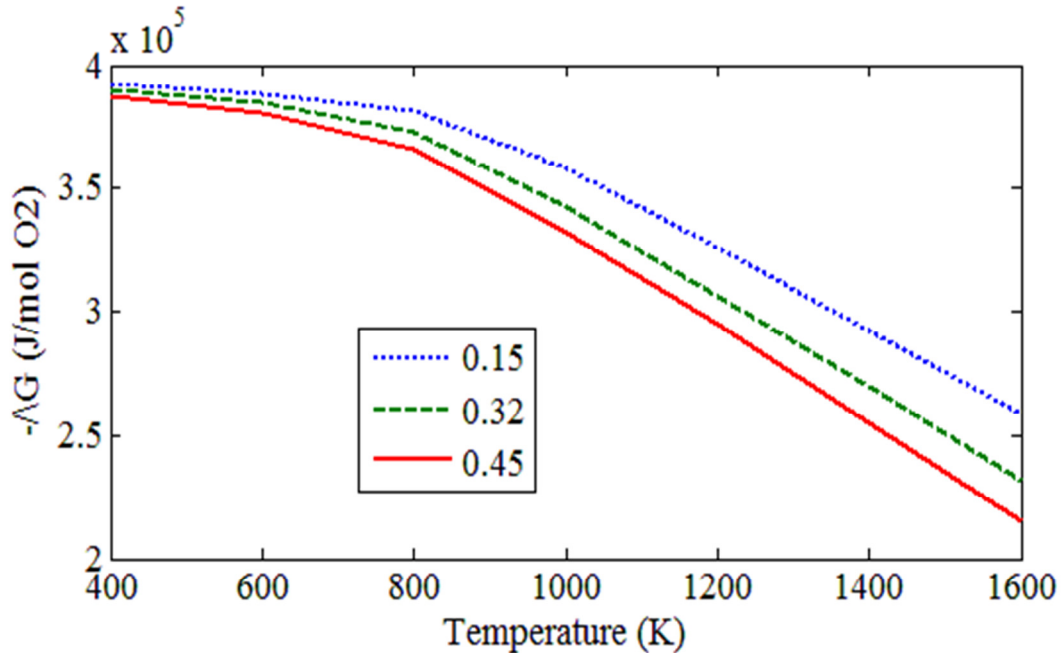
**Figure 4-14:** Gibbs free energy per mole oxygen as a function of temperature for the following molecular amounts of oxygen: 0.15 $O_2$, 0.32 $O_2$, and 0.45 $O_2$ in the original biomass composition. As the amount of oxygen in the biomass increases, the Gibbs free energy decreases.

As can be seen in **Figure 4-14**, the fuel's oxygen content proves to be detrimental to fuel cell performance. Gibbs free energy is shown to decrease as the oxygen content in the biomass increases. Studies have shown that bio-oil typically contains an oxygen to carbon ration of 0.5, while gasoline and diesel have a zero value for this ratio [48]. According to **Figure 4-14,** if biomass with significantly high oxygen content is used as feedstock going into the reactor, then deoxygenation must take place in some part of the gasifier in order to achieve optimal output. As mentioned before, however, deoxygenation is not always favored due to the fact that it often results in consummation of the initial reserve of carbon and hydrogen.

The reactor favors fast pyrolysis in order to prevent biochar from being produced over bio-oil and syngas; this proves to be detrimental to the byproduct due the fact that most of the biomass's internal oxygen is being transformed into water in the form of liquid [49]. Byproducts of slow pyrolysis have been shown to have less oxygen content due to secondary reactions of dehydration, decarbonization, and condensation. It is thus a compromise between fast pyrolysis and slow pyrolysis. Fast pyrolysis will yield less biochar and more syngas with higher oxygen content while sow pyrolysis will yield more biochar with smaller amounts of syngas with low oxygen content.

As mentioned before, hydrodeoxygenation is a common technology used to remove oxygen from biomass at the expense of lowering hydrogen content. However, the oxygen content can only be decreased to as low as 2-5 wt.% [48]. Thus, these processes are only used when the proper catalyst can be introduced in order to remove oxygen without causing any significant change to the original composition. Introducing catalysts, such as CoMoP, to hydrotreated biomass can yield 90% reduction in oxygen content without having to sacrifice hydrogen content. This catalyst has consequently been shown to double the heating value of the hydrotreated biomass [48]. Although the introduction of these catalysts is very complex, they nonetheless show promise for future implementation of deoxygenation into the gasification process. Biomass is already two steps ahead of coal in the sense that it is renewable and requires less combustion in the gasifier due to its higher oxygen content. With the assistance of deoxygenation, biomass can gain that extra step towards higher overall performance over coal.

## 4.7    Temperature Difference between Reactor and Fuel Cell

Thus far, all of the data computed in previous sections had assumed that the reactor and fuel cell are kept at the same temperature. Realistically, however, the temperature of the reactor will be kept at a temperature below the fuel cell. Based on the composition graphs shown in section 4.1, hydrogen content is shown at peak at about 1000 K for all three cases. The goal is to achieve optimal hydrogen concentration of the syngas leaving the reactor and entering the fuel cell. By keeping the temperature of that reactor constant at 1000 K and varying the temperature difference between the reactor and fuel cell, we were able to calculate the max power density, or MPD, of the fuel cell. The MPD is plotted as a function of the SOFC temperature, as can be seen in **Figure 4-13**:
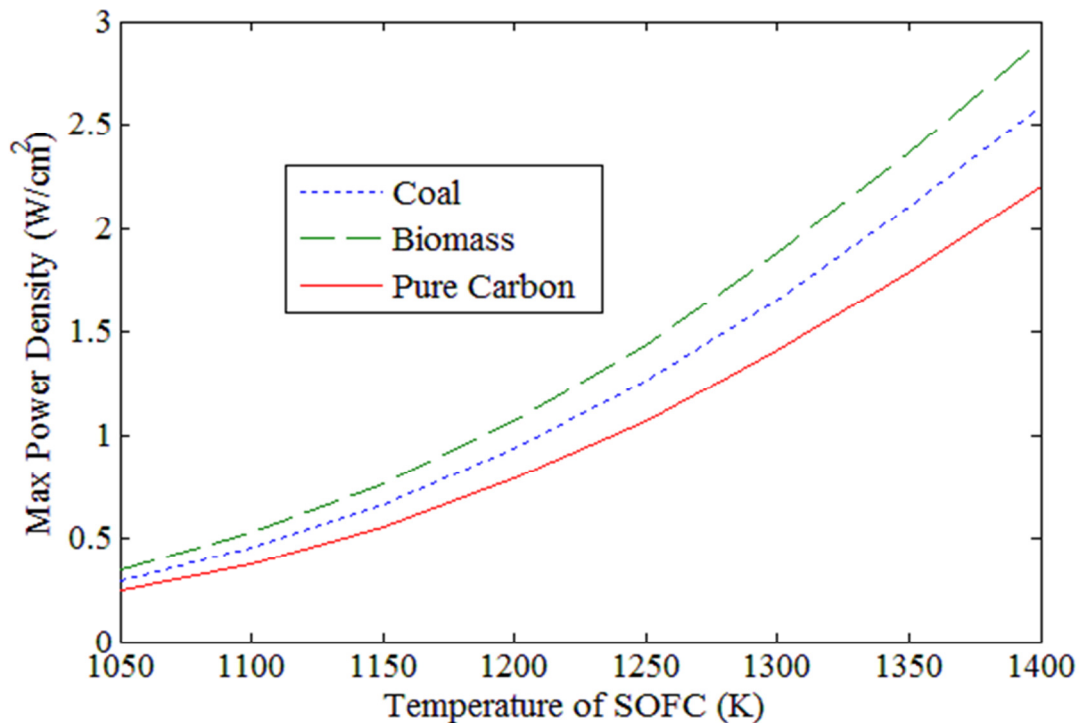


**Figure 4-13**: Max power density as a function of SOFC temperature for pure carbon, coal, and biomass. The temperature of the reactor is fixed at 1000 K and the temperature difference between the reactor and SOFC is carried out in increments of 50 K. Max Power density

76

increases as the temperature difference increases. The SOFC should be kept at a temperature well above the reactor temperature. Pure carbon has the highest MPD while biomass has the lowest MPD for any given SOFC temperature.

As can be seen in **Figure 4-13**, the temperature difference, or $\Delta T$, is carried out in increments of 50 K. The code used to create this figure can be seen in Appendix I. The MPP increases as $\Delta T$ increases. Thus, the temperature of the SOFC should be kept at a temperature well above the temperature of the reactor to increase power performance. Pure carbon-derived syngas still attains the highest MPP for any given temperature, while biomass-derived syngas once again has the lowest performance. Similar to **Figure 4-12**, the current density increases as the MPP increases. Thus, higher MPP can be achieved at higher temperatures at the expense of using more current density. The key difference between **Figure 4-15** and **Figure 4-12** is the maximum power point at 1400 K. For pure carbon-derived syngas, for example, the power peaks at 2.8 $\frac{W}{cm^2}$ when the SOFC temperature is at 1400 K and the reactor is fixed at 1000 K. When the reactor is kept at the same temperature as the SOFC, however, the power peaks at 4.2 $\frac{W}{cm^2}$ at a temperature of 1400 K. It can thus be said that the energy required to heat the fuel cell inlet gases from the reactor temperature to the SOFC temperature outweighs the benefit of having syngas with optimal hydrogen concentration entering the fuel cell.

## CONCLUSIONS

SOFCs are considered as promising energy conversion devices for converting a fuel, such as syngas, to heat and electricity due to its advantages such as its ability to

integrate with external gasifiers, high power performance, syngas composition flexibility, and low greenhouse gas emissions. In this thesis, we modeled the thermodynamic energy for an external reforming SOFC coupled with a biomass-to-syngas reactor. We based the composition of the syngas output from the reactor on temperature and feedstock being used. We analyzed four different feedstocks for their fuel cell heat dissipation and fuel cell power characteristics: pure syngas, pure carbon-derived syngas, coal-derived syngas, and biomass-derived syngas. Pure syngas was the only case that did not take the reactor into account; the syngas output was assumed to consist of only hydrogen and carbon monoxide. The syngas output for pure carbon, coal, and biomass was assumed to consist of hydrogen, carbon monoxide, carbon dioxide, methane, and water. Specific values vary based on the specific fuel cell being used during actual experimentation. For this reason, we placed greater emphasis on trends rather than specific values. After analyzing the results section of this thesis, we found there to be five major outcomes that can further the research of a biomass-to-syngas reactor coupled with an SOFC.

1) In order to calculate the maximum power density and heat dissipation of the SOFC, we had to initially analyze the Gibbs free energy and voltage in order to further understand the thermodynamics of the fuel cell process. Since pure syngas did not take the reactor into account, a separate Gibbs free energy analysis was conducted for this feedstock. The results had shown the Gibbs free energy of the fuel cell for pure syngas to increase as the hydrogen concentration increased for temperatures above 1100 K. For temperatures below 1100 K, Gibbs free energy increased as the hydrogen concentration decreased due to the chemical system having much lower entropy change at lower temperatures than at higher temperatures. A separate analysis, which took into account the reactor, involved the other three feedstocks. The results of the energy analysis of the reactor had shown the biomass to have the highest change in Gibbs free energy, followed by

coal and pure carbon. This consequently caused the change in the Gibbs free energy of the fuel cell for biomass to be very small. The results of the energy analysis of the fuel cell had shown pure carbon to have the highest change in Gibbs free energy. Polarization curves for all four cases had shown that ohmic and activation losses became less significant as the temperature increased.

2) The characteristics seen in the polarization curves inherently affected the power performance for all four cases; a higher maximum power point (MPP) was achieved at higher temperatures due to the voltage losses becoming less and less significant. Results from the maximum power density section had shown pure syngas to have the highest MPP for any given temperature, followed by pure carbon, coal, and biomass. The only downside to operating at higher temperatures is that the MPP can only be achieved via high current density. Thus, concentration losses would have to be accounted for at these higher temperatures. Since these higher temperatures are impractical, the thermodynamic model used in this thesis did not account for mass transport.

3) The second outcome assumed the reactor and fuel cell are kept at the same temperature; this third outcome assumes the fuel cell and reactor to be at different temperatures. Optimal concentration of syngas entering the fuel cell would have a higher concentration of hydrogen above anything else in order to ensure that water and carbon dioxide are the only products of the fuel cell. The results of the equilibrium composition analysis had shown pure carbon to achieve the highest amount of hydrogen at any given reactor temperature, followed by coal and biomass. Nonetheless, the composition graphs had shown hydrogen concentration to be at its highest for all three cases at a reactor temperature of about 1000 K. A separate study had shown that if the reactor temperature is kept constant at 1000

K while the SOFC temperature is kept at a higher temperature, the MPP at any given temperature would not be as high as the case in which the reactor is kept at the same temperature as the SOFC. The energy required to heat the fuel cell inlet gases from the reactor temperature to the SOFC temperature outweighs the benefit of delivering optimal hydrogen concentrated syngas to the SOFC.

4) Heat dissipation of the fuel cell was also calculated in addition to power performance for the case of pure carbon, coal, and biomass. As temperature increased, the enthalpy of reaction for the reactor steadily decreased and the heat released from the fuel cell increased. No energy in the form of work had to be redirected to generating heat from the fuel cell; heat transferred to the environment due to reaction in the fuel cell exceeded that required for the endothermic reactions in the reactor. Thus, the results section of this thesis ultimately displayed pure carbon to dissipate the most heat and generate the most electrical work, followed by coal and biomass. Pure carbon was oxygen-free before the reactor and hydrogen-rich after the reactor, thus allowing for much higher overall performance.

5) A separate study had shown that high oxygen content hindered the performance of biomass, thus requiring the incorporation of de-oxygenation in the reactor. Without de-oxygenation, the use of coal would give overall better performance over biomass at the cost of more ash and more burning of air. The use of biomass would require less burning of air and release less ash at the cost of lower work performance and lower heat deliverance. By using the proper technique of de-oxygenation in a gasifier, biomass has the potential to achieve higher overall performance over coal.

**LIST OF REFERENCES**

[1] http://www.epa.gov/Sustainability/ Date Accessed: March 21, 2011

[2] http://bioenergy.ornl.gov/papers/bioam95/graham3.html Date Accessed: March 24, 2011

[3] Alyaser, M., Beitelmal, A., Monaghan, R., and Fabris, D. Introducing a Novel Reactor Concept: Indirectly Fired Integrated Gasification and Steam Generation System. Proceedings of the ASME 2010 International Mechanical Engineering Congress & Exposition, November 12-18, 2010.

[4] Lattin, W.C., and Utgikar, V.P.. Transition to hydrogen economy in the United States: A 2006 status report. International Journal of Hydrogen Energy, Volume 32, Issue 15, October 2007, Pages 3230-3237.

[5] Marbán, G., and Valdés-Solís, T.. Towards the hydrogen economy? International Journal of Hydrogen Energy, Volume 32, Issue 12, February 2007, Pages 1625-1637.

[6] Edwards, P.P. , Kuznetsov, V.L., David, W.I.F., and Brandon, N.P.. Hydrogen and fuel cells: Towards a sustainable energy future. Energy Policy, Volume 36, Issue 12, May 2008, Pages: 4356-4362

[7] International Energy Agency (IEA). Moving to a hydrogen economy: dreams and realities. IEA/SLT 5. 2003.

[8] http://csis.org/files/media/csis/pubs/0510gsifuturewatchhydrogen.pdf Date Accessed: March 28, 2011

[9] http://www1.eere.energy.gov/biomass/pdfs/sustainability_four_pager.pdf Date Accessed: March 25, 2011

[10] http://image.guardian.co.uk/sys-files/Environment/documents/2008/01/18/EACbiofuelsreport.pdf Date Accessed: April 21, 2011

[11] http://bioenergy.ornl.gov/papers/bioam95/graham3.html Date Accessed: March 23, 2011

[12] http://www.internationaltransportforum.org/jtrc/DiscussionPapers/DiscussionPaper3.pdf Date Accessed: March 23, 2011

[13] Balat, M., and Balat, M.. Political, economic and environmental impacts of biomass-based hydrogen. International Journal of Hydrogen Energy, Volume 34, Issue 9, May 2009, Pages 3589-3603.

[14] http://www.getenergysmart.org/files/hydrogeneducation/6hydrogenproductionsteammethanereforming.pdf Date Accessed: March 24, 2011

[15]  http://www.unep.fr/energy/information/publications/factsheets/pdf/cogeneration.pdf Date Accessed: March 23, 2011

[16]  Alanne, K, Saari, A., Ugursal, V.I., and Good, J..  The financial viability of an SOFC cogeneration system in single-family dwellings. Journal of Power Sources, Volume 158, Issue 1, July 2006, Pages 403-416.

[17]  Beausoleil-Morrison, I., and Lombardi, K. The calibration of a model for simulating the thermal and electrical performance of a 2.8kWAC solid-oxide fuel cell micro-cogeneration device. Journal of Power Sources, Volume 186, Issue 1, January 2009, Pages 67-79.

[18]  Ferguson, A., and Ugursal, V.I.. Fuel cell modeling for building cogeneration applications. Journal of Power Sources, Volume 137, Issue 1, October 2004, Pages 30-42.

[19]  Krumdieck, S., Page, S., and Round, S.. Solid oxide fuel cell architecture and system design for secure power on an unstable grid. Journal of Power Sources, Volume 125, Issue 2, January 2004, Pages 189-198.

[20]  Mac, E., Gray, A., Webb, C.J., Andrews, J., Shabani, B., Tsai, P.J., and Chan, S.L.I.. Hydrogen storage for off-grid power supply. International Journal of Hydrogen Energy, Volume 36, Issue 1, January 2011, Pages 654-663.

[21]  http://www.sbg.ac.at/ipk/avstudio/pierofun/fuelcell/fuelcell.html Date Accessed: April 21, 2011

[22]  Igot, F.. Face Off: Internal Combustion Engine versus the Hydrogen Fuel Cell. Montgomery College Student Journal of Science and Mathematics, Volume 1, September 2002.

[23]  Zamel, N., and Li, X.. Life cycle comparison of fuel cell vehicles and internal combustion engine vehicles for Canada and the United States. Journal of Power Sources, Volume 162, Issue 2, November 2006, Pages 1241-1253.

[24]  http://www.brighthub.com/engineering/mechanical/articles/18082.aspx?p=2 Date Accessed: April 21, 2011

[25]  Dea, S., and Assadib, M.. Impact of co-firing biomass with coal in power plants – A techno-economic assessment. Biomass and Bioenergy, Volume 33, Issue 2, February 2009, Pages 283-293.

[26]  http://www.nrel.gov/docs/fy00osti/28009.pdf Date Accessed: April 23, 2011

[27]    http://pubs.cas.psu.edu/FreePubs/PDFs/ub044.pdf Date Accessed: March 31, 2011

[28]    http://www.fossil.energy.gov/programs/powersystems/gasification/index.html Date Accessed: April 14, 2011

[29]    http://www.fischer-tropsch.org/DOE/DOE_reports/igccbro/igccbro.pdf Date Accessed: April 11, 2011

[30]    Li, M., Rao, A., Brouwer, J., and Samuelsen, S.. Design of highly efficient coal-based integrated gasification fuel cell power plants. Journal of Power Sources, Volume 195, Issue 17, September 2010, Pages 5707-5718.

[31]    http://www.uaex.edu/Other_Areas/publications/PDF/FSA-1052.pdf Date Accessed: April 9, 2011

[32]    Asadullah, M., Rahman, M.A., Ali, M.M., Rahman, M.S., Motin, M.A., Sultan, M.B., and Alam, M.R.. Production of bio-oil from fixed bed pyrolysis of bagasse. Fuel, Volume 86, Issue 16, November 2007, Pages 2514-2520.

[33]    Demirbas, A. Combustion characteristics of different biomass fuels. Progress in Energy and Combustion Science, Volume 30, Issue 2, 2004, Pages 219-230.

[34]    http://www.cpeo.org/techtree/ttdescript/pyrols.htm Date Accessed: April 4, 2011

[35]    http://www.altenergymag.com/emagazine.php?issue_number=09.02.01&article=pyrolysis Date Accessed: April 21, 2011

[36]    Van de Weerdhof, M.W. Modeling the pyrolysis process of biomass particles. The Canadian Journal of Chemical Engineering, Volume 69, Issue 4, August 1991, Pages 907–915.

[37]    Rajvanshi, A. Biomass Gasification. Alternative Energy in Agriculture, Volume 2, 1986, Pages 83-102.

[38]    Colpan, C.O.. Thermal Modeling of Solid Oxide Fuel Cell Based Biomass Gasification Systems. Carleton University, DAI-B 71/05, 2009.

[39]    Brammer, J.G., and Bridgwater, A.V.. Drying technologies for an integrated gasification bio-energy plant. Renewable and Sustainable Energy Reviews, Volume 3, Issue 4, December 1999, Pages 243-289.

[40]    Boerrigter, H., and Rauch, R.. Review of applications of gases from biomass gasification. Handbook Biomass Gasification, Chapter 10, June 2006.

[41]    Ciferno, J.P., and Marano, J.J.. Benchmarking Biomass Gasification Technologies for Fuels, Chemicals and Hydrogen Production. U.S. Department of Energy National Energy Technology Laboratory, June 2002.

[42]    Ciferno, J.P., and Marano, J.J.. Benchmarking Biomass Gasification
        Technologies for Fuels, Chemicals and Hydrogen Production. U.S.
        Department of Energy National Energy Technology Laboratory, June 2002.

[43]    Rajvanshi, A. Biomass Gasification. Alternative Energy in Agriculture,
        Volume 2, 1986, Pages 83-102.

[44]    Ryan, P., Cha, S., and Colella, W.. Fuel cell fundamentals. Wiley, New
        York, 2009.

[45]    Colpana, C.O., Dincerb, I., and Hamdullahpura, F.. Thermodynamic
        modeling of direct internal reforming solid oxide fuel cells operating with
        syngas. International Journal of Hydrogen Energy, Volume 32, Issue 7, May
        2007, Pages 787-795.

[46]    Sordi, A., da Silva, E.P., Neto, A.J.M., Lopes, D.G., Pinto, C.S., and
        Araújo, P.D.. Thermodynamic Simulation of Biomass Gas Steam Reforming
        for a Solid Oxide Fuel Cell (SOFC) System. Brazilian Journal of Chemical
        Engineering, Volume 26, Issue 04, December, 2009, Pages 745 – 755.

[47]    Ciferno, J.P., and Marano, J.J.. Benchmarking Biomass Gasification
        Technologies for Fuels, Chemicals and Hydrogen Production. U.S.
        Department of Energy National Energy Technology Laboratory, June 2002.

[48]    Bulushev, D.A., and Ross, J.. Catalysis for conversion of biomass to fuels
        via pyrolysis and gasification: A review. Catalysis Today, Volume 171, Issue
        1, August 2011, Pages 1-13.

[49]    Luik, H., Johannes, I., Palu, V., Luik, L., and Kruusement, K..
        Transformations of biomass internal oxygen at varied pyrolysis conditions.
        Journal of Analytical and Applied Pyrolysis, Volume 79, Issues 1-2, May
        2007, Pages 121-127.

**APPENDICES**

# APPENDIX A: PURE SYNGAS REVERSIBLE CELL VOLTAGE

```matlab
function [Eo] = revcellvoltage(T1,P1,x)


gas1 = GRI30; %%% Water
set(gas1,'T',T1,'P',P1,'X','H2O:1');
hmole1 = enthalpy_mole(gas1);
smole1 = entropy_mole(gas1);
hmass1 = entropy_mass(gas1);
gibb1 = x*(hmole1-(T1*smole1));

gas2 = GRI30; %%%% Carbon Dioxide
set(gas2,'T',T1,'P',P1,'X','CO2:1');
hmole2 = enthalpy_mole(gas2);
smole2 = entropy_mole(gas2);
gibb2 = (1-x)*(hmole2-(T1*smole2));

gas3 = GRI30; %%% Carbon Monoxide
set(gas3,'T',T1,'P',P1,'X','CO:1');
hmole3 = enthalpy_mole(gas3);
smole3 = entropy_mole(gas3);
gibb3 = (1-x)*(hmole3-(T1*smole3));

gas4 = GRI30; %%% Air
set(gas4,'T',T1,'P',P1,'X','O2:.21,N2:.79');
hmole4 = enthalpy_mole(gas4);
smole4 = entropy_mole(gas4);
gibb4 = 0.5*(hmole4-(T1*smole4));

gas5 = Hydrogen;
set(gas5,'T',T1,'P',P1);
hmole5 = enthalpy_mole(gas5);
smole5 = entropy_mole(gas5);
gibb5 = x*(hmole5-(T1*smole5));

gibb6 = 8314*T1*log(1/(((.21*P1)/101325)^.5));

totalgibb = ((gibb1+gibb2)-(gibb3+gibb4+gibb5)+gibb6)/1000; %% J/mol

F = 96400; %%% Faraday Constant (C/mol)
n = 2;

Eo = totalgibb/(-n*F);
```

# APPENDIX B: COAL, BIOMASS, AND PURE CARBON  REVERSIBLE CELL VOLTAGE

```matlab
function [totalgibb] = realrevcellvoltage(T1,P1,h,co,w,co2,ch4)

x = (co+co2+ch4); % water produced
y = ((2*h)+(2*w)+(4*ch4))/2; %carbon dioxide produced
z = ((2*x)+y-co-w-(2*co2))/2; %oxygen required for stoichiometric
display(z)

%%Reactants
gas1 = Hydrogen;
gas2 = GRI30; %%% Carbon Monoxide
gas3 = GRI30; %%% Water
gas4 = GRI30; %%%% Carbon Dioxide
gas5 = Methane;
gas6 = Oxygen;
%%Products
gas7 = GRI30; %%% Carbon Dioxide
gas8 = GRI30; %%% Water


set(gas1,'T',T1,'P',P1);
hmole1 = enthalpy_mole(gas1);
smole1 = entropy_mole(gas1);
gibb1 = h*(hmole1-(T1*smole1));

set(gas2,'T',T1,'P',P1,'X','CO:1');
hmole2 = enthalpy_mole(gas2);
smole2 = entropy_mole(gas2);
gibb2 = co*(hmole2-(T1*smole2));

set(gas3,'T',T1,'P',P1,'X','H2O:1');
hmole3 = enthalpy_mole(gas3);
smole3 = entropy_mole(gas3);
gibb3 = w*(hmole3-(T1*smole3));

set(gas4,'T',T1,'P',P1,'X','CO2:1');
hmole4 = enthalpy_mole(gas4);
smole4 = entropy_mole(gas4);
gibb4 = co2*(hmole4-(T1*smole4));

set(gas5,'T',T1,'P',P1);
hmole5 = enthalpy_mole(gas5);
smole5 = entropy_mole(gas5);
```

```
gibb5 = ch4*(hmole5-(T1*smole5));

set(gas6,'T',T1,'P',P1);
hmole6 = enthalpy_mole(gas6);
smole6 = entropy_mole(gas6);
gibb6 = z*(hmole6-(T1*smole6));

set(gas7,'T',T1,'P',P1,'X','CO2:1');
hmole7 = enthalpy_mole(gas7);
smole7 = entropy_mole(gas7);
gibb7 = x*(hmole7-(T1*smole7));

set(gas8,'T',T1,'P',P1,'X','H2O:1');
hmole8 = enthalpy_mole(gas8);
smole8 = entropy_mole(gas8);
gibb8 = y*(hmole8-(T1*smole8));

logg =
(((y*(P1/101325))^y)*((x*(P1/101325))^x))/(((ch4*(P1/101325))^ch4)*((h*
(P1/101325))^h)*((co*(P1/101325))^co)*((w*(P1/101325))^w)*((co2*(P1/101
325))^co2)*((z*(P1/101325))^z));

gibb9 = 8314*T1*log(logg);

totalgibb = (((((gibb7+gibb8)-
(gibb1+gibb2+gibb3+gibb4+gibb5+gibb6)+gibb9)/1000))/z; %% J/(mol O2)
```

# APPENDIX C: PURE SYNAS ENTHALPY OF REACTION

```matlab
function [deltah] = enthalpy(T1,P1,x)


gas1 = GRI30; %%% Water
set(gas1,'T',T1,'P',P1,'X','H2O:1');
hmole1 = enthalpy_mole(gas1);
smole1 = entropy_mole(gas1);

gas2 = GRI30; %%%% Carbon Dioxide
set(gas2,'T',T1,'P',P1,'X','CO2:1');
hmole2 = enthalpy_mole(gas2);
smole2 = entropy_mole(gas2);

gas3 = GRI30; %%% Carbon Monoxide
set(gas3,'T',T1,'P',P1,'X','CO:1');
hmole3 = enthalpy_mole(gas3);
smole3 = entropy_mole(gas3);

gas4 = GRI30; %%% Air
set(gas4,'T',T1,'P',P1,'X','O2:.21,N2:.79');
hmole4 = enthalpy_mole(gas4);
smole4 = entropy_mole(gas4);
gibb4 = 0.5*(hmole4-(T1*smole4));

gas5 = Hydrogen;
set(gas5,'T',T1,'P',P1);
hmole5 = enthalpy_mole(gas5);
smole5 = entropy_mole(gas5);

%%% deltah = x*(h,f + h@T1 - h@298K)H2O + (1-x)*(h,f + h@T1 -
h@298K)CO2 -
%%% (1-x)*(h,f + h@T1 - h@298K)CO - .5*(0 + h@T1 - h@298K)O2 - x*(0 +
%%% h@T1 - h@298K)H2

deltah = ((x*(-241820000+(hmole1+2.4183e+008)))+((1-x)*(-
393520000+(hmole2+3.9351e+008)))-((1-x)*(-
110530000+(hmole3+1.1053e+008)))-(.5*(hmole4+12092))-
(x*(hmole5+3505)))/1000; %% J/mol
```

# APPENDIX D: COAL, BIOMASS, AND PURE CARBON ENTHALPY OF REACTION

```
function [deltah] = realenthalpy(T1,P1,h,co,w,co2,ch4)

x = (co+co2+ch4); % water produced
y = ((2*h)+(2*w)+(4*ch4))/2; %carbon dioxide produced
z = ((2*x)+y-co-w-(2*co2))/2; %oxygen required for stoichiometric
display(z)

%%Reactants
gas1 = Hydrogen;
gas2 = GRI30; %%% Carbon Monoxide
gas3 = GRI30; %%% Water
gas4 = GRI30; %%%% Carbon Dioxide
gas5 = Methane;
gas6 = Oxygen;
%%Products
gas7 = GRI30; %%% Carbon Dioxide
gas8 = GRI30; %%% Water


set(gas1,'T',T1,'P',P1);
hmole1 = enthalpy_mole(gas1);

set(gas2,'T',T1,'P',P1,'X','CO:1');
hmole2 = enthalpy_mole(gas2);

set(gas3,'T',T1,'P',P1,'X','H2O:1');
hmole3 = enthalpy_mole(gas3);

set(gas4,'T',T1,'P',P1,'X','CO2:1');
hmole4 = enthalpy_mole(gas4);

set(gas5,'T',T1,'P',P1);
hmole5 = enthalpy_mole(gas5);

set(gas6,'T',T1,'P',P1);
hmole6 = enthalpy_mole(gas6);

set(gas7,'T',T1,'P',P1,'X','CO2:1');
hmole7 = enthalpy_mole(gas7);

set(gas8,'T',T1,'P',P1,'X','H2O:1');
```

```matlab
hmole8 = enthalpy_mole(gas8);

%%% deltah = x*(h,f + h@T1 - h@298K)H2O + (1-x)*(h,f + h@T1 -
h@298K)CO2 -
%%% (1-x)*(h,f + h@T1 - h@298K)CO - .5*(0 + h@T1 - h@298K)O2 - x*(0 +
%%% h@T1 - h@298K)H2
deltah = (((y*(-241820000+(hmole8+2.4183e+008)))+((x)*(-
393520000+(hmole7+3.9351e+008)))-((co)*(-
110530000+(hmole2+1.1053e+008)))-(z*(hmole6+12092))-(h*(hmole1+3505))-
(w*(-241820000+(hmole3+2.4183e+008)))-((co2)*(-
393520000+(hmole4+3.9351e+008)))-(ch4*hmole5))/1000)/z; %% J/(mol O2)
```

# APPENDIX E: ACTIVATION LOSS

```matlab
function [activation_overvoltage] = actover(T1,c)

F = 96400;                      %%% Faraday Constant (C/mol)
n = 2;                          %%% number of electrons tranferred
R = 8.314;                      %%% universal gas constant (J/mol*K)
jo = .001;                      %%% universal gas constant (J/mol*K)

alpha = .5;                     %%% transport coefficient
j(c) = c/100;                   %%% current density (A/cm^2)
                                %%% area of fuel cell assumed to be 100
cm^2

j_bv = @(activation_overvoltage)
(jo*(exp(((alpha*n*F*activation_overvoltage)/(R*T1))) - exp((((alpha-
1)*n*F*activation_overvoltage)/(R*T1)))));

activation_overvoltage(c) = fzero(@(x) j_bv(x) - j(c),1);
```

# APPENDIX F: OHMIC LOSS

```matlab
function [ohmic_overvoltage] = ohmover(T1,c)


L1 = .005;          %%% thickness of electrode membrane (cm)
L2 = .001;          %%% thickness of electrolyte membrane (cm)
A = 100;            %%% electrolyte constant (K/m*sigma)
j = (.01*c)-0.01;   %%% current density (A/cm^2) assuming Area of fuel
cell = 100 cm^2
%j=c/A;
F = 96400;          %%% Faraday Constant (C/mol)
z1 = 1;             %%% amount of charge carried by charged species
across electrode
z2 = 2;             %%% amount of charge carried by charged species
across electrolyte
q = 1.602*10^-19;   %%% electron charge (C)
m = 9.11*10^-31;    %%% mass of electron (kg)
c1 = 1;             %%% molar concentration of charge carries in
electrode (mol/cm^3)
c2 = .1;            %%% molar concentration of charge carriers in
electrolyte (mol/cm^3)
tao = 10^-13;       %%% mean free time between scattering (s)
R = 8.314;          %%% universal gas constant (J/mol*K)
D = 10^-8;          %%% Diffusivity of polymer electrolyte (m^2/s)
G = 90000;          %%% electrolyte activation energy (J/mol)


conductivity_electrode = (z1*F*c1*q*tao)/(m);

conductivity_electrolyte = 900*((A*exp(-G/(R*T1))))/T1;



ohmic_overvoltage = j*((L1/conductivity_electrode)
+(L2/conductivity_electrolyte));
```

# APPENDIX G: VOLTAGE

```
function Vfc = voltage(T1,P1,x,c)

f2 = actover(T1,c);
f1 = revcellvoltage(T1,P1,.4);
f3 = ohmover(T1,c);

jx=.01.*c;
Vfc = f1-activation_overvoltage-f3;
```

# APPENDIX H: PEAK POWER

```
Tarray = linspace(600,1400,41);

for T = 1:41
    T_j = Tarray(T)

    for c = 1:1:1200


        F = 96400;
        n = 2;
        R = 8.314;
        jo = (8.66*10^7)*exp(-22082/T_j);
        alpha = .5;
        j(c) = (.01*c)-0.01;

        j_bv = @(activation_overvoltage)
(jo*(exp(((alpha*n*F*activation_overvoltage)/(R*T_j))) - exp((((alpha-
1)*n*F*activation_overvoltage)/(R*T_j)))));

        activation_overvoltage(c) = fzero(@(x) j_bv(x) - j(c),1);

    end
        c = 1:1:1200;
        f3 = ohmover(T_j,c);
        f1 = revcellvoltage(T_j,oneatm,.5);



        jx=(.01*c)-.01;
        Vfc = f1-activation_overvoltage-f3;
        Pd=Vfc.*jx;
        b = polyfit(jx,Pd,10);
        bp = polyder(b);
        maxjx = roots(bp)
        maxjx(maxjx<0)=[]
        maxjx(maxjx>13)=[]
        g = maxjx(imag(maxjx)==0)
        maxpd(T) = polyval(b,g)
        maxpd(maxpd<0)=[]


end
```

# APPENDIX I: PEAK POWER FOR FIXED REACTOR TEMPERATURE

```matlab
%% q1, q2, and q3 = energy required to heat fuel cell inlet gases from
reactor temperature to SOFC temperature.
Q = mcp/\T. Since m = 1 mol and /\h(T) = cp/\T for ideal gases, Q = /\h

Tarray = linspace(50,400,8);

for T = 1:8
    T_j = Tarray(T)
    Td = T_j+1000;

    for c = 1:1:1200


        F = 96400;
        n = 4;
        R = 8.314;
        jo = (8.66*10^7)*exp(-22082/Td);
        alpha = .5;
        j(c) = (.01*c)-0.01;



        j_bv = @(activation_overvoltage)
(jo*(exp(((alpha*n*F*activation_overvoltage)/(R*Td))) - exp((((alpha-
1)*n*F*activation_overvoltage)/(R*Td)))));

        activation_overvoltage(c) = fzero(@(x) j_bv(x) - j(c),1);

    end
        c = 1:1:1200;
        jx=(.01*c)-.01;

        f3 = ohmover(Td,c);


        %%% Coal
        g1 = GRI30;
        x1 =
set(g1,'T',1000,'P',2*oneatm,'X','C:.34,H2:.026,O2:.058,N2:.006,H2O:.51
');
        x2 = equilibrate(g1,'TP');
```

```matlab
        h2 = moleFraction(x2, 'H2');
        h2o = moleFraction(x2, 'H2O');
        co2 = moleFraction(x2, 'CO2');
        co = moleFraction(x2, 'CO');
        ch4 = moleFraction(x2, 'CH4');
        f1 = realrevcellvoltage(Td,oneatm,h2,co,h2o,co2,ch4);
        q1 = realenthalpy(Td,oneatm,h2,co,h2o,co2,ch4);
        Vfc = f1-activation_overvoltage-f3-q1;
        Pd=Vfc.*jx;
        b = polyfit(jx,Pd,10);
        bp = polyder(b);
        maxjx = roots(bp);
        maxjx(maxjx<0)=[];
        maxjx(maxjx>16)=[];
        g = maxjx(imag(maxjx)==0)
        maxpd(T) = polyval(b,g);
        maxpd(maxpd<0)=[];

        %%% Biomass
        g2 = GRI30;
        x2a =
set(g2,'T',1000,'P',2*oneatm,'X','C:.32,H2:.035,O2:.17,N2:.005,H2O:.47'
);
        x2b = equilibrate(g2,'TP');
        h2b = moleFraction(x2b, 'H2');
        h2ob = moleFraction(x2b, 'H2O');
        co2b = moleFraction(x2b, 'CO2');
        cob = moleFraction(x2b, 'CO');
        ch4b = moleFraction(x2b, 'CH4');
        f1b = realrevcellvoltage(Td,oneatm,h2b,cob,h2ob,co2b,ch4b);
        q2 = realenthalpy(Td,oneatm,h2b,cob,h2ob,co2b,ch4b);
        Vfcb = f1b-activation_overvoltage-f3-q2;
        Pdb=Vfcb.*jx;
        bb = polyfit(jx,Pdb,10);
        bpb = polyder(bb);
        maxjxb = roots(bpb);
        maxjxb(maxjxb<0)=[];
        maxjxb(maxjxb>16)=[];
        gb = maxjxb(imag(maxjxb)==0)
        maxpdb(T) = polyval(bb,gb);
        maxpdb(maxpdb<0)=[];

        %%% Pure Carbon
        g3 = GRI30;
        x3a = set(g3,'T',1000,'P',2*oneatm,'X','C:.4,H2O:.6');
        x2c = equilibrate(g3,'TP');
        h2c = moleFraction(x2c, 'H2');
        h2oc = moleFraction(x2c, 'H2O');
```

```matlab
        co2c = moleFraction(x2c, 'CO2');
        coc = moleFraction(x2c, 'CO');
        ch4c = moleFraction(x2c, 'CH4');
        f1c = realrevcellvoltage(Td,oneatm,h2c,coc,h2oc,co2c,ch4c);
        q3 = realenthalpy(Td,oneatm,h2c,coc,h2oc,co2c,ch4c);
        Vfcc = f1c-activation_overvoltage-f3-q3;
        Pdc=Vfcc.*jx;
        bc = polyfit(jx,Pdc,10);
        bpc = polyder(bc);
        maxjxc = roots(bpc);
        maxjxc(maxjxc<0)=[];
        maxjxc(maxjxc>17)=[];
        gc = maxjxc(imag(maxjxc)==0)
        maxpdc(T) = polyval(bc,gc);
        maxpdc(maxpdc<0)=[];


end

k = 1:8;
plot(k,maxpd,k,maxpdb,k,maxpdc)
xlabel('Temperature (K)')
ylabel('Max Power Density (W/cm^2)')
legend('Coal','Biomass','Pure Carbon')
```